
De-randomizing MCMC dynamics with the diffusion Stein operator

Zheyang Shen Markus Heinonen Samuel Kaski

Department of Computer Science
Aalto University, Finland
first.last@aalto.fi

Abstract

Approximate Bayesian inference estimates descriptors of an intractable target distribution – in essence, an optimization problem within a family of distributions. For example, Langevin dynamics (LD) extracts asymptotically exact samples from a diffusion process because the time evolution of its marginal distributions constitutes a curve that minimizes the KL-divergence via steepest descent in the Wasserstein space. Parallel to LD, Stein variational gradient descent (SVGD) similarly minimizes the KL, albeit endowed with a novel Stein-Wasserstein distance, by *deterministically* transporting a set of particle samples, thus de-randomizes the stochastic diffusion process. We propose de-randomized kernel-based particle samplers to all diffusion-based samplers known as MCMC dynamics. Following previous work in interpreting MCMC dynamics, we equip the Stein-Wasserstein metric with a fiber-Riemannian Poisson structure, with the capacity of characterizing a fiber-gradient Hamiltonian flow that simulates MCMC dynamics. Such dynamics discretize into generalized SVGD (GSVGD), a Stein-type deterministic particle sampler, with particle updates coinciding with applying the *diffusion Stein operator* to a kernel function. We demonstrate empirically that GSVGD can de-randomize complicated MCMC dynamics, which combine the advantages of auxiliary momentum variables and Riemannian structure, while maintaining the high sample quality from an interacting particle system.

1 Introduction

Evaluating an un-normalized target distribution π is a centerpiece of Bayesian inference, due to its ubiquitous presence in posterior distributions. Markov chain Monte Carlo (MCMC) methods fulfill this objective by generating asymptotically exact random samples from the distribution, a significant subset of which involves discretization of continuous-time diffusion processes, most notably Langevin diffusion, stochastic gradient Hamiltonian Monte Carlo (HMC) (Chen et al., 2014) and their further generalizations, which we collectively call MCMC *dynamics* (Ma et al., 2015). Despite its simplicity and theoretical soundness, this diffusion-based sampling often suffers from slow convergence and small effective sample sizes, largely due to the auto-correlation of the samples.

As an alternative to the simulation of stochastic systems, particle-based variational inference (Liu and Wang, 2016; Chen et al., 2018; Liu et al., 2019a) partially addresses the shortcomings of MCMC by replacing the Langevin diffusion, the simplest MCMC dynamics, with a deterministic interacting particle system that transports a set of interacting particles towards the target distribution. Theoretically speaking, Langevin diffusion encodes an evolution of density that minimizes the KL-divergence through steepest descent in the 2-Wasserstein space (Jordan et al., 1998), and particle-based variational inference (PARVI) approximates such evolution using reproducing kernel Hilbert space (RKHS) (Liu, 2017; Liu et al., 2019a), thus de-randomizing the Langevin diffusion process.

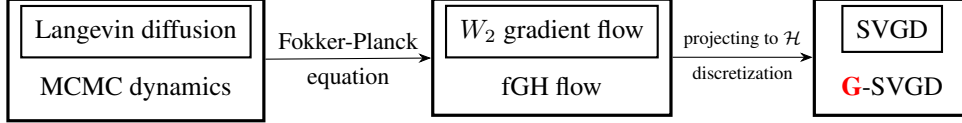


Figure 1: A diagram showing the contribution of our paper: we extend and generalize previous work linking Langevin diffusion to gradient flow on the 2-Wasserstein metric W_2 through the Fokker-Planck equation, and the W_2 gradient flow linking to SVGD (Liu and Wang, 2016) through projection onto an RKHS; MCMC dynamics (Ma et al., 2015) are interpreted as a fiber-gradient Hamiltonian (fGH) flow on W_2 (Liu et al., 2019b), and a projection onto an RKHS yields GSVGD.

Given the elegant theoretical link between Langevin diffusion and PARVI, one crucial question arises: can we leverage the advantages of general MCMC dynamics onto de-randomized particle systems? While it is difficult to formulate them as a direct Wasserstein gradient flow, Liu et al. (2019b) propose an interpretation for “regular” MCMC dynamics that augments the 2-Wasserstein space with a fiber bundle, forming a fiber-Riemannian Poisson manifold, under which MCMC dynamics follows a Hamiltonian flow on the fiber bundle, and a gradient flow on each fiber.

We show that adapting the fiber-Riemannian Hamiltonian flow to the Stein-Wasserstein metric (Liu, 2017; Duncan et al., 2019) yields a vector field in the form of applying the *diffusion Stein operator* to the kernel function $k(\cdot, \theta)$. A discretization of this vector field gives generalized SVGD (GSVD), an interacting particle system that generalizes SVGD, with particle updates balancing an attractive force maximizing the log-likelihood and a repulsive force preventing a “mode collapse” of particles. We further demonstrate that the connection drawn between LD and SVGD (Liu and Wang, 2016; Liu, 2017; Liu et al., 2019a) is retraced by GSVGD, reaffirming our claim that GSVGD mirrors SVGD in approximating a larger class of MCMC diffusion processes. Within the generality of our framework, we can develop PARVI algorithms that exploit two key types of possible acceleration in MCMC dynamics: auxiliary momentum variables and an adaptive Riemannian parametrization that allows for fast and efficient exploration of the probability space (Girolami and Calderhead, 2011), as shown in Table 1.

MCMC dynamics	A	C	auxiliary variable	Riemannian	PARVI variant
SGLD (Welling and Teh, 2011)	I	0	✗	✗	SVGd (Liu and Wang, 2016)
SGRLD (Girolami and Calderhead, 2011)	$G(\theta)^{-1}$	0	✗	✓	Blob (Chen et al., 2018)
SGHMC (Chen et al., 2014)	$\begin{pmatrix} 0 & 0 \\ 0 & \mathbf{I} \end{pmatrix}$	$\begin{pmatrix} 0 & -\mathbf{I} \\ \mathbf{I} & 0 \end{pmatrix}$	✓	✗	Riemannian SVGD (Liu and Zhu, 2017)
SGRHMC (Ma et al., 2015)	$\begin{pmatrix} 0 & 0 \\ 0 & G(\theta)^{-1} \end{pmatrix}$	$\begin{pmatrix} 0 & -G(\theta)^{-1/2} \\ G(\theta)^{-1/2} & 0 \end{pmatrix}$	✓	✓	HMC-blob (Liu et al., 2019b)
					this work (SGRHMC-Stein)

Table 1: An overview of MCMC dynamics along with their PARVI approximations. Between (a), (c) and (b), (d), MCMC dynamics are stochastic single-chain simulations of a diffusion process (shown by one instance of a particle trajectory); PARVI approximates the time evolution of MCMC densities with a set of particles with deterministic dynamics; Between (a), (b) and (c), (d), the two systems follows different time evolutions, as (a), (b) describe a gradient flow and (c), (d) describe a fiber-gradient Hamiltonian flow (with momentum variable r).

2 MCMC dynamics – the relevant bits

In this paper, we consider the problem of extracting samples $\theta \in \mathbb{R}^D = \Omega$ from an un-normalized target distribution $\pi(\theta) \propto e^{-H(\theta)}$. We begin by reviewing the key characteristics of MCMC dynamics, with particular emphasis on Langevin dynamics and its Fokker-Planck equation (FPE), the partial differential equation (PDE) that depicts the time evolution of a diffusion process. As the

FPE of LD conforms to a gradient flow structure in the 2-Wasserstein metric space of probability measures $(\mathcal{P}(\Omega), W_2)$ (Jordan et al., 1998), we then briefly cover gradient flow on $\mathcal{P}(\Omega)$ as an infinite-dimensional Riemannian manifold. Through the lens of gradient flow, we can see SVGD as a deterministic interacting particle system that approximates the gradient flow of LD through (i) gradient flow on a novel Stein-Wasserstein metric (Liu, 2017) or (ii) projecting the gradient flow direction onto an RKHS (Liu et al., 2019a). With Wasserstein gradient flow (WGF) neatly linking to both LD and SVGD, we see that a diffusion process LD and an interacting particle system SVGD are, respectively, a stochastic instance and a deterministic approximation of the same Wasserstein gradient flow.

Notations: We use ∇f to denote the gradient of a scalar-valued function, and $\nabla \cdot \mathbf{f}$ the divergence of a vector-valued function, $\nabla \cdot \mathbf{A}$ applies the divergence operator to each row of a matrix-valued function, $\dot{\rho}_t$ the ‘‘partial derivative’’ with respect to t .

2.1 Langevin dynamics and its Fokker-Planck equation

In this paper, we consider MCMC dynamics in the form of Itô diffusion processes following the stochastic differential equation (SDE) formula

$$d\boldsymbol{\theta}_t = \mathbf{f}(\boldsymbol{\theta}_t)dt + \sqrt{2\Sigma(\boldsymbol{\theta}_t)}d\mathbf{W}_t, \quad (1)$$

consisting of drift coefficient $\mathbf{f} : \mathbb{R}^D \mapsto \mathbb{R}^D$, diffusion coefficient $\sqrt{2\Sigma}$ and a D -dimensional Brownian motion \mathbf{W}_t . Ma et al. (2015) provide a complete recipe of all Itô diffusion processes converging to the target measure π . The simplest MCMC dynamics takes the form of Langevin diffusion (Langevin, 1908), which moves towards higher densities with $\mathbf{f}(\boldsymbol{\theta}) = \nabla \log \pi(\boldsymbol{\theta})$ perturbed by white noise $\Sigma = \mathbf{I}$. Given an initial distribution $\boldsymbol{\theta}_0 \sim \rho_0$, the Fokker-Planck equation describes the time evolution of the density of $\boldsymbol{\theta}_t$ (Risken, 1996)

$$\dot{\rho}_t + \nabla \cdot (\rho_t \nabla \log \pi) - (\nabla \nabla) : (\rho_t \mathbf{I}) = 0, \quad (2)$$

where $\mathbf{X} : \mathbf{Y} = \text{tr}(\mathbf{X} \top \mathbf{Y})$. Given that $(\nabla \nabla) : \mathbf{M} = \nabla \cdot (\nabla \cdot \mathbf{M})$, we can rewrite (2) as

$$\dot{\rho}_t = \nabla \cdot (\nabla \rho_t - \rho_t \nabla \log \pi) = \nabla \cdot \left(\rho_t \nabla \underbrace{\frac{\delta \text{KL}[\rho_t \parallel \pi]}{\delta \rho_t}}_{\text{first variation of KL}[\rho_t \parallel \pi]} \right), \quad (3)$$

a crucial step in developing the Wasserstein gradient flow perspective of LD, as $\nabla \delta E / \delta \rho$ coincides with the differential of functionals induced by the Wasserstein metric.

2.2 Gradient flow on $(\mathcal{P}(\Omega), W_2)$

The conventional gradient flow (or the steepest descent curve) that minimizes a smooth function $F : \mathbb{R}^D \mapsto \mathbb{R}$ follows the PDE: $\dot{\mathbf{x}}_t + \nabla F(\mathbf{x}_t) = 0$. Defining gradient flow on $\mathcal{P}(\Omega)$, informally written as $\dot{\rho}_t + \nabla_W E(\rho_t) = 0$, requires a definition of the differentiation ∇_W , which requires an understanding of the Wasserstein metric, i.e., the inner product g_ρ defined on its tangent space.

To simplify the discussion, we restrict the discussion on measures with a density function and with finite second-order moments. For each ρ , the tangent space constitutes smooth functions integrating to zero, $T_\rho \mathcal{P}(\Omega) = \{f | f \in C^\infty(\Omega), \int f(\boldsymbol{\theta})d\boldsymbol{\theta} = 0\}$, in that a curve on $\mathcal{P}(\Omega)$ preserves volume. The cotangent space constitutes an equivalence class of smooth functions in differing constant, noted as the quotient space $T_\rho^* \mathcal{P}(\Omega) = C^\infty(\Omega)/\mathbb{R}$. We characterize the inner product space using the metric tensor $G(\rho) : T_\rho \mathcal{P} \mapsto T_\rho^* \mathcal{P}$, a one-to-one mapping between elements of the tangent space and those of the cotangent space. The inner product g_ρ is defined by the inverse of the metric tensor, often denoted as Onsager operators (Onsager, 1931)

$$g_\rho(f_1, f_2) = \int f_1 G(\rho) f_2 d\boldsymbol{\theta} = \int \phi_1 G(\rho)^{-1} \phi_2 d\mathbf{x}, \quad \phi_1 = G(\rho) f_1, \quad \phi_2 = G(\rho) f_2. \quad (4)$$

The Wasserstein Onsager operator takes the form $G(\rho)^{-1} : \phi \mapsto -\nabla \cdot (\rho \nabla \phi)$. In the context of Wasserstein gradient flow, we define $\nabla_W E(\rho)$ as $G(\rho)^{-1} \frac{\delta E(\rho)}{\delta \rho}$, leading to the formulation:

$$0 = \dot{\rho}_t - G(\rho)^{-1} \frac{\delta E(\rho_t)}{\delta \rho_t} = \dot{\rho}_t + \nabla \cdot \left(\rho_t \nabla \frac{\delta E(\rho_t)}{\delta \rho_t} \right). \quad (5)$$

The first variation of $\text{KL}[\rho \parallel \pi]$ takes the form of $\frac{\delta \text{KL}[\rho \parallel \pi]}{\delta \rho} = \log \rho / \pi + 1$, leading to the conclusion by [Jordan et al. \(1998\)](#) that the time evolution of the Langevin diffusion follows a curve of steepest descent in the Wasserstein space, laying the foundation for approximation using particle interaction.

2.3 SVGD as gradient flow

PARVI transports a set N of interacting particles $\{\theta_t^{(i)}\}_{1 \leq i \leq N}$ towards the target distribution over time. Take SVGD for example, denoting the empirical measure at time t as $\hat{\rho}_t = \frac{1}{N} \sum_{i=1}^N \delta_{\theta_t^{(i)}}$, SVGD ([Liu and Wang, 2016](#)) follows the update rule

$$\dot{\theta}_t = \mathbb{E}_{\theta' \sim \hat{\rho}_t} \left[k(\theta_t, \theta') \nabla \log \pi(\theta') + \nabla_2 k(\theta_t, \theta') \right] = \mathbf{v}_{\mathcal{H}}(\theta_t | \hat{\rho}_t), \quad (6)$$

where $k(\cdot, \cdot)$ defines a positive-definite kernel, and ∇_2 denotes the gradient of the second argument. The FPE of SVGD can be written as

$$\dot{\rho}_t - \nabla \cdot \left(\rho_t \mathcal{K}_\rho \nabla \frac{\delta \text{KL}[\rho_t \parallel \pi]}{\delta \rho_t} \right) = 0, \quad (7)$$

where \mathcal{K}_ρ is an integral operator: $\mathcal{K}_\rho \mathbf{f}(\theta) = \int k(\theta, \theta') \mathbf{f}(\theta') d\rho(\theta')$. We shall denote the RKHS defined by k as \mathcal{H} . While significantly different from LD at first glance, SVGD approximates the WGF of LD by

- kernelizing the Wasserstein Onsager operator to give $G_{\mathcal{H}}(\rho)^{-1} : \phi \mapsto -\nabla \cdot (\rho \mathcal{K}_\rho \nabla \phi)$, thus forming the Stein-Wasserstein metric $W_{\mathcal{H}}$ ([Liu, 2017](#); [Duncan et al., 2019](#));
- projecting the gradient flow vector field $\mathbf{v}(\rho) = -\nabla \frac{\delta \text{KL}[\rho \parallel \pi]}{\delta \rho} = \nabla \log \pi - \nabla \log \rho$ onto \mathcal{H} ([Liu et al., 2019a](#)).

The interpretation of SVGD yields valuable insights. While gradient flow (7) on $(\mathcal{P}(\Omega), W_2)$ yields no closed-form energy functional ([Chen et al., 2018](#)), it behooves to absorb the operator \mathcal{K}_ρ into the definition of the Stein-Wasserstein metric to guarantee a tractable energy functional. In the meantime, the kernelization trick transforms a gradient flow (2) simulated by a diffusion process into an approximate deterministic transportation of particles – in other words, de-randomizes it.

2.4 MCMC dynamics as fiber-gradient Hamiltonian flow

The concept of *flow* on $(\mathcal{P}(\Omega), W_2)$ is a generalization of the gradient flow: given a vector field $\mathbf{v} : \mathcal{P}(\Omega) \mapsto \bigcup_{\rho \in \mathcal{P}} T_\rho$, the flow of \mathbf{v} is defined as $\dot{\rho}_t = \mathbf{v}(\rho_t)$. [Liu et al. \(2019b\)](#) interpret “regular” MCMC dynamics on $(\mathcal{P}(\Omega), W_2)$ as a flow, by combining gradient flow and Hamiltonian flow on the Wasserstein space, yielding a fiber-Riemannian manifold structure of $\mathcal{P}(\Omega)$, a fiber bundle consisting of Riemannian manifolds. In the context of a “regular” MCMC dynamics taking the form of underdamped Langevin dynamics ([Chen et al., 2014](#)), the diffusion matrix \mathbf{A} determines the gradient flow on each fiber, and the curl matrix \mathbf{C} determines the Hamiltonian flow on the fiber bundle. The Hamiltonian flow keeps $\text{KL}[\rho \parallel \pi]$ constant while encouraging fast exploration of the probability space; the fiber gradient flow minimizes the KL. The fiber-gradient Hamiltonian flow determines a PARVI with the particle update

$$\dot{\theta}_t = (\mathbf{A}(\theta_t) + \mathbf{C}(\theta_t)) \left(\nabla \log \pi(\theta_t) - \widehat{\nabla} \log \rho_t(\theta_t) \right) = \mathbf{v}^{\mathbf{A}, \mathbf{C}}(\rho_t), \quad (8)$$

where the intractable $\widehat{\nabla} \log \rho_t$ is approximated via the Blob method ([Carrillo et al., 2019](#)).

2.5 Stein’s method and other relevant works

Our work enriches the practical application of Stein’s method ([Stein, 1972](#)), which studies the class of operators that maps functions to ones with expectation zero w.r.t. a distribution π . [Gorham et al. \(2019\)](#) draw from the findings of the generator method ([Barbour, 1988, 1990](#); [Gotze, 1991](#)) and note the same property with infinitesimal generators of Feller processes and their stationary measures, which further extends into a mapping between diffusion-based MCMC sampling and Stein operators, noted as *diffusion Stein operators*. In this work, we extend beyond sample quality measurement

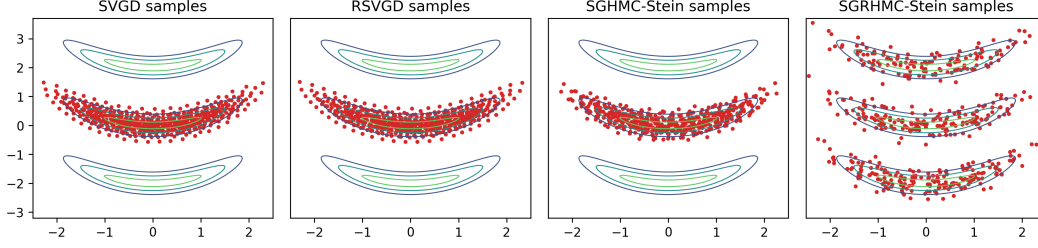


Figure 2: Particle samples of an underlying 2-dimensional correlated mixture π extracted by SVGD (Liu and Wang, 2016), Riemannian SVGD (Liu and Zhu, 2017), SGHMC-Stein and SGRHMC-Stein. While all methods explore the mode nearest to initialization, only RHMC explores all three modes.

(Gorham et al., 2019) and parameter estimation (Barp et al., 2019) and establish an application of the diffusion Stein operator as a deterministic alternative of MCMC dynamics.

Myriad works (Chen et al., 2018; Liu et al., 2019a; Zhang et al., 2020) seek alternatives to approximating the gradient flow (2) through kernelization. Notably, Chen et al. (2018); Liu et al. (2019a) construct PARVI algorithms by approximating the term $\nabla \log \rho_t(\theta_t)$ in the gradient flow, namely with Blob method (Carrillo et al., 2019), kernel density estimation (Liu et al., 2019a) and Stein gradient estimator (Li and Turner, 2017). The de-randomization of underdamped LD connects to the viewpoint of accelerating PARVI methods. Ma et al. (2019) demonstrate that underdamped LD (Chen et al., 2014) accelerates the steepest descent steps taken by the overdamped LD, forming an analog of Nesterov acceleration for MCMC methods. Wang and Li (2019) present a framework for Nesterov’s accelerated gradient method in the Wasserstein space, which consists of augmenting the energy functional with the kinetic energy of an additional momentum variable.

3 PARVI for MCMC dynamics – a general recipe

In this section, we outline the main contribution of this work, which traces the roadmap delineated by previous works to explore the flow interpretation, as well as the approximation by interacting particle systems of general form MCMC dynamics (Ma et al., 2015) in the form of Itô diffusion:

$$\mathbf{f}(\boldsymbol{\theta}) = \frac{1}{\pi(\boldsymbol{\theta})} \nabla \cdot [\pi(\boldsymbol{\theta}) (\mathbf{A}(\boldsymbol{\theta}) + \mathbf{C}(\boldsymbol{\theta}))], \quad (9)$$

$$\boldsymbol{\Sigma}(\boldsymbol{\theta}) = \mathbf{A}(\boldsymbol{\theta}), \quad (10)$$

where \mathbf{A} and \mathbf{C} are positive-semidefinite and skew-symmetric matrix-valued functions, respectively. This general framework covers *all* continuous Itô diffusion processes with stationary distribution π , most notably LD, stochastic gradient HMC (Chen et al., 2014), stochastic gradient Nosé-Hoover thermostat (SGNHT) (Ding et al., 2014) and stochastic gradient Riemannian Hamiltonian Monte Carlo (SGRHMC) (Ma et al., 2015).

We demonstrate in this section that applying the fiber-gradient Hamiltonian flow structure of MCMC dynamics to the Stein-Wasserstein metric yields a flow on $(\mathcal{P}(\Omega), W_{\mathcal{H}})$ that discretizes into GSVG, a PARVI that updates particles with the diffusion Stein operator (Gorham et al., 2019), suggesting that the infinitesimal generator of MCMC diffusion processes offers a “kernel smoothing” de-randomization. Apart from the Stein-Wasserstein metric, the analog of GSVG generalizing SVGD extends to other interpretations of SVGD, namely that GSVG takes steepest descent minimizing the KL-divergence in incremental transformation of particles, and that that GSVG projects the fiber-gradient Hamiltonian flow onto an RKHS.

3.1 Fiber-gradient Hamiltonian flow on $(\mathcal{P}(\Omega), W_{\mathcal{H}})$

Similar to (2), we derive the FPE of MCMC dynamics (9)-(10)

$$\dot{\rho}_t = -\nabla \cdot (\rho_t \mathbf{f}) + (\nabla \nabla) : (\rho_t \mathbf{A}) \quad (11)$$

$$= -\nabla \cdot (\rho_t \mathbf{f}) + (\nabla \nabla) : (\rho_t \mathbf{A}) + \underbrace{(\nabla \nabla) : (\rho_t \mathbf{C})}_{=0} \quad (12)$$

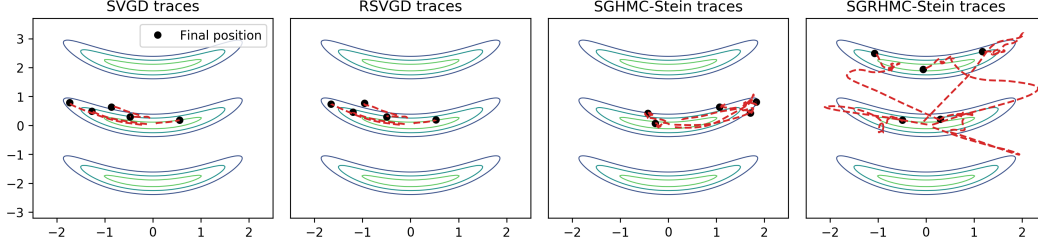


Figure 3: A visualisation of sampler trajectories on the tri-Gaussian density π . With the help of momentum variable and efficient Riemannian parametrization of (\mathbf{A}, \mathbf{C}) , SGRHMC-Stein aggressively explores the space, while other methods cannot escape the local component.

$$= \nabla \cdot \left(\rho_t (\mathbf{A} + \mathbf{C}) \nabla \log \frac{\rho_t}{\pi} \right) = \nabla \cdot \left(\rho_t (\mathbf{A} + \mathbf{C}) \nabla \frac{\delta \text{KL}[\rho_t \parallel \pi]}{\delta \rho_t} \right), \quad (13)$$

which is a curve in $\mathcal{P}(\Omega)$ following the continuity equation $\dot{\rho}_t + \nabla \cdot (\rho_t \mathbf{v}_t) = 0$, $\mathbf{v}_t = (\mathbf{A} + \mathbf{C}) \nabla \log \rho_t / \pi$.

We can derive GSVG from the fiber-Riemannian manifold perspective of $(\mathcal{P}(\Omega), W_{\mathcal{H}})$ (Liu et al., 2019b). The Riemannian structure of the Stein-Wasserstein metric induces the tangent space $T_{\rho} \mathcal{P}(\Omega) = \overline{\{\mathcal{K}_{\rho} \nabla f \mid f \in C^{\infty}(\Omega)\}}^{\mathcal{H}^D}$. An orthogonal projection \mathfrak{p}_{ρ} from $\mathcal{L}_{\rho}^2(\Omega)$ to $T_{\rho} \mathcal{P}$ is uniquely defined as such vector in $T_{\rho} \mathcal{P}$ that satisfies $\nabla \cdot (\rho \mathcal{K}_{\rho} \phi) = \nabla \cdot (\rho \mathfrak{p}_{\rho}(\phi))$. Using Theorem 5 from Liu et al. (2019b), we arrive at a fiber-gradient Hamiltonian flow

$$\mathcal{W}_{\text{KL}\pi}(\rho) = \mathfrak{p}_{\rho}((\mathbf{A} + \mathbf{C}) \nabla \log \pi / \rho). \quad (14)$$

It is straightforward to verify that $\mathbf{v}_{\mathcal{H}}^{\mathbf{A}, \mathbf{C}}(\rho) = \mathcal{K}_{\rho}(\mathbf{A} + \mathbf{C}) \nabla \log \pi / \rho$ induces the same evolution of distribution as $\mathcal{W}_{\text{KL}\pi}(\rho)$.

3.2 FRH flow induces the diffusion Stein operator

The Wasserstein flow on $(\mathcal{P}(\Omega), W_{\mathcal{H}})$ following $\dot{\rho}_t = \nabla \cdot (\rho_t \mathbf{v}_{\mathcal{H}}^{\mathbf{A}, \mathbf{C}}(\rho_t))$ requires spatial and temporal discretization suitable for a particle update. While $\mathbf{v}_{\mathcal{H}}^{\mathbf{A}, \mathbf{C}}$ constitutes a vector field on $\mathcal{P}(\Omega)$, its calculation does not involve an explicit term of $\nabla \log \rho$ inside the expectation.

$$\mathbf{v}_{\mathcal{H}}^{\mathbf{A}, \mathbf{C}}(\rho) = \mathcal{K}_{\rho}[(\mathbf{A} + \mathbf{C}) \nabla \log \pi / \rho] \quad (15)$$

$$\begin{aligned} &= \mathbb{E}_{\theta' \sim \rho} k(\cdot, \theta') (\mathbf{A}(\theta') + \mathbf{C}(\theta')) \nabla \log \pi(\theta') - \int k(\cdot, \theta') (\mathbf{A}(\theta') + \mathbf{C}(\theta')) \nabla \rho(\theta') d\theta' \\ &= \mathbb{E}_{\theta' \sim \rho} (\mathbf{A}(\theta') + \mathbf{C}(\theta')) \nabla \log \pi(\theta') k(\cdot, \theta') + \underbrace{\int \nabla \cdot ((\mathbf{A}(\theta') + \mathbf{C}(\theta')) k(\cdot, \theta')) d\rho}_{\text{integration by parts}} \\ &= \mathbb{E}_{\theta' \sim \rho} \left[\underbrace{\mathbf{f}(\theta') k(\cdot, \theta')}_{\text{weighted drift coefficient (9)}} + \underbrace{(\mathbf{A} + \mathbf{C})(\theta') \nabla_2 k(\cdot, \theta')}_{\text{repulsive force}} \right]. \end{aligned} \quad (16)$$

$$= \mathbb{E}_{\theta' \sim \rho} \underbrace{\frac{1}{\pi} \nabla \cdot (\pi (\mathbf{A} + \mathbf{C}) k(\cdot, \theta'))}_{\text{diffusion Stein operator } \mathcal{T}_{\pi}^{\mathbf{A}, \mathbf{C}} k(\cdot, \theta')}, \quad (17)$$

where ∇_2 refers to the gradient w.r.t. the second argument of the kernel function. Interestingly, the kernelized flow $\mathbf{v}_{\mathcal{H}}^{\mathbf{A}, \mathbf{C}}$ coincides with calculating the expectation of the diffusion Stein operator $\mathcal{T}_{\pi}^{\mathbf{A}, \mathbf{C}}$ (Gorham et al., 2019) applied to the kernel function $k(\theta, \cdot)$, a family of operators mapping functions to zero-expectation functions under an (un-normalized) distribution π . When ρ_t is approximated by the empirical measure of its particles $\hat{\rho}_t = 1/N \sum_{i=1}^N \delta_{\theta_t^{(i)}}$, we can derive the particle update of

$$\dot{\theta}_t = \mathbf{v}_{\mathcal{H}}^{\mathbf{A}, \mathbf{C}}(\hat{\rho}_t) = \mathbb{E}_{\theta' \sim \hat{\rho}_t} \mathcal{T}_{\pi}^{\mathbf{A}, \mathbf{C}} k(\theta_t, \theta') = \frac{1}{N} \sum_{i=1}^N \mathcal{T}_{\pi}^{\mathbf{A}, \mathbf{C}} k(\theta_t, \theta_t^{(i)}), \theta_0^{(i)} \sim \rho_0. \quad (18)$$

Similar to SVGD, the particle update of GSVGd leverages between a weighted average of the drift vector and a repulsive force, which drives particles towards the target distribution while preventing a mode collapse. The fiber-gradient Hamiltonian flow on $(\mathcal{P}(\Omega), W_{\mathcal{H}})$ informs a duality between diffusion Stein operator and MCMC dynamics, extending the use of Stein operators beyond a generalization of kernel Stein discrepancy (Gorham et al., 2019).

3.3 How does GSVGd approximate MCMC dynamics?

While the derivation of GSVGd originates from the flow interpretation on $W_{\mathcal{H}}$, the analogy between SVGd and GSVGd expresses in equivalent alternative forms discussed by previous literature, further shedding light on the interpretation of GSVGd.

Originally, the SVGd update is expressed in the form of the functional gradient (Liu and Wang, 2016). For MCMC dynamics, we similarly derive the functional gradient with respect to the push-forward measure $\rho_\epsilon = (\text{id} + (\mathbf{A} + \mathbf{C})^\top \mathbf{v})_{\#} \rho, \mathbf{v} \in \mathcal{H}^D$,

$$\nabla_{\mathbf{v}} \text{KL}[\rho_\epsilon \parallel \pi] |_{\mathbf{v}=\mathbf{0}} = -\mathbb{E}_{\boldsymbol{\theta}' \sim \rho} \mathcal{T}_{\pi}^{\mathbf{A}, \mathbf{C}} k(\cdot, \boldsymbol{\theta}') = -\mathbf{v}_{\mathcal{H}}^{\mathbf{A}, \mathbf{C}}(\rho). \quad (19)$$

This presents a generalization of the discussion in Liu and Wang (2016) that GSVGd takes incremental transformation of particles in the direction that minimizes KL-divergence, with such transformation warped by (\mathbf{A}, \mathbf{C}) and constrained by RKHS.

Alternatively, Liu et al. (2019a) explains SVGd as the projection of the original gradient flow direction $\mathbf{v}(\rho_t) = \nabla \log \pi / \rho_t$ onto an RKHS. We similarly generalize this explanation for SVGd, as it projects $\mathbf{v}_{\mathcal{H}}^{\mathbf{A}, \mathbf{C}}(\rho_t) = (\mathbf{A} + \mathbf{C}) \nabla \log \pi / \rho_t \in \mathcal{L}_{\rho}^2$ onto \mathcal{H}^D , as

$$\mathbf{v}_{\mathcal{H}}^{\mathbf{A}, \mathbf{C}}(\rho) = \max_{\mathbf{v} \in \mathcal{H}^D, \|\mathbf{v}\|_{\mathcal{H}^D}=1} \arg \max \langle \mathbf{v}_{\mathcal{H}}^{\mathbf{A}, \mathbf{C}}(\rho), \mathbf{v} \rangle_{\mathcal{L}_{\rho}^2}. \quad (20)$$

The analogy of GSVGd goes further when we consider the transportation of N particles as inferring a joint distribution $\pi^{\otimes N}$, which will be covered in the supplements.

3.4 GSVGd in practice

We can apply GSVGd updates (16) to de-randomize myriad MCMC dynamics (e.g., Table 1). Notably, GSVGd establishes the previously unexplored duality between Riemannian Langevin diffusion (Girolami and Calderhead, 2011) and Riemannian SVGd (Liu and Zhu, 2017).

To fully harness the capacity of our framework, we can introduce auxiliary (momentum) variables \mathbf{r} to help with the exploration of probability space, namely to augment the target distribution as $\pi(\boldsymbol{\theta}, \mathbf{r}) = \pi(\boldsymbol{\theta}) \mathcal{N}(\mathbf{r} | \mathbf{0}, \boldsymbol{\Sigma})$, therefore achieving de-randomized PARVI variant of stochastic gradient Hamiltonian Monte Carlo (SGHMC) (Chen et al., 2014). Further leveraging a positive definite $\mathbf{G}(\boldsymbol{\theta})$ to efficiently explore the target distribution yields a PARVI variant of SGRHMC (Ma et al., 2015).

When GSVGd is used in conjunction with auxiliary momentum variables, we can employ symmetric splitting for leapfrog-like steps for GSVGds de-randomizing with momentum,

$$\mathbf{r}_{k+1/2}^{(i)} = \mathbf{r}_k^{(i)} + \frac{\epsilon}{2} \mathbf{v}_{\mathcal{H}}^{\mathbf{A}, \mathbf{C}} \left(\mathbf{r}_k^{(i)} \mid \hat{\rho}(\boldsymbol{\theta}_k, \mathbf{r}_k) \right), \quad (21)$$

$$\boldsymbol{\theta}_{k+1}^{(i)} = \boldsymbol{\theta}_k^{(i)} + \epsilon \mathbf{v}_{\mathcal{H}}^{\mathbf{A}, \mathbf{C}} \left(\boldsymbol{\theta}_k^{(i)} \mid \hat{\rho}(\boldsymbol{\theta}_k, \mathbf{r}_{k+1/2}) \right), \quad (22)$$

$$\mathbf{r}_{k+1}^{(i)} = \mathbf{r}_{k+1/2}^{(i)} + \frac{\epsilon}{2} \mathbf{v}_{\mathcal{H}}^{\mathbf{A}, \mathbf{C}} \left(\mathbf{r}_{k+1/2}^{(i)} \mid \hat{\rho}(\boldsymbol{\theta}_{k+1}, \mathbf{r}_{k+1/2}) \right). \quad (23)$$

4 Experiments

4.1 Stein PARVI on toy data

To demonstrate the efficacy of our methods, we use various PARVI to infer a 3-component mixture of crescent-shaped target measure inspired by Ma et al. (2015). The parametrizations of Riemannian SVGd and SGRHMC-Stein coincide with those in Ma et al. (2015). While all methods explore the nearest mode well (See figure 2), only the SGRHMC-Stein manage to effectively use the Riemannian formulation of (\mathbf{A}, \mathbf{C}) to explore the 2 other modes (see figure 3), showcasing the gain in efficiency with application-specific dynamics.

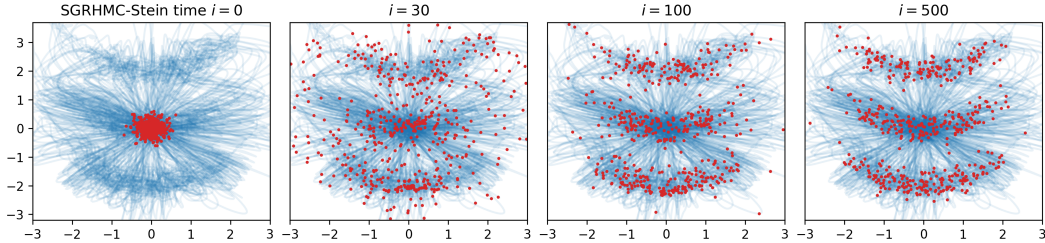


Figure 4: Evolution of RHM dynamics (blue lines) over four highlighted time increments k (red points) on tri-Gaussian density. The RHM explores the space by an aggressive outward expansion followed by convergence to the tri-Gaussian density π .

4.2 GSVG D on Bayesian neural networks

We apply GSVG D of advanced MCMC dynamics to the inference of Bayesian neural networks, taking a simple structure of one hidden layer, and an output with Gaussian likelihood. We opt for the fully Bayesian specification of BNN, where the precision parameter of the weight prior and the Gaussian likelihood follows Gamma(1, 0.1). The GSVG D variant used in the experiments include SGHMC (Chen et al., 2014) and SGNHT (Ding et al., 2014), with target measure $\pi(\theta, \mathbf{r}, \xi) = \pi(\theta)\mathcal{N}(\mathbf{r}|\mathbf{0}, \sigma^2\mathbf{I})\mathcal{N}(\xi|A\mathbf{1}, \mu^{-1}\mathbf{I})$, and $\mathbf{A} = \begin{pmatrix} \mathbf{0} & \mathbf{0} & \mathbf{0} \\ \mathbf{0} & A\mathbf{I} & \mathbf{0} \\ \mathbf{0} & \mathbf{0} & \mathbf{0} \end{pmatrix}$, $\mathbf{C} =$

$$\begin{pmatrix} \mathbf{0} & -\mathbf{I} & \mathbf{0} \\ \mathbf{I} & \mathbf{0} & (\mu\sigma^2)^{-1}\text{diag}(\mathbf{r}) \\ \mathbf{0} & -(\mu\sigma^2)^{-1}\text{diag}(\mathbf{r}) & \mathbf{0} \end{pmatrix}. \text{ As a MCMC form suitable when used in conjunc-}$$

tion with stochastic gradients, SGNHT takes additional temperature parameter ξ . The log-likelihood results in Table 2 demonstrates that the de-randomized MCMC dynamics achieve superior predictive performance than their LD counterparts, largely thanks to the exploration of probability space from the momentum variables (See figure 5), with a notable gain from symmetric splitting. SGNHT-Stein methods show robustness to hyperparameter selection and stochastic gradient noise.

5 Discussion

In this section, we discuss open questions pertinent to the ‘‘optimality’’ of the diffusion Stein operator as a PARVI update, and a direction for future work regarding the fiber-gradient Hamiltonian flow of the chi-squared divergence, inspired by Chewi et al. (2020).

5.1 Alternatives to the diffusion Stein operator

The vector field $\mathbf{v}^{\mathbf{A}, \mathbf{C}}(\rho) = (\mathbf{A} + \mathbf{C}) \nabla \log \frac{\pi}{\rho}$ is not the unique vector field that induces the time evolution of MCMC dynamics: indeed, two vector fields $\mathbf{v}_1, \mathbf{v}_2$ induce the same curve in $\mathcal{P}(\Omega)$ when they differ by a divergence-free field: $\nabla \cdot (\rho(\mathbf{v}_1(\rho) - \mathbf{v}_2(\rho))) = 0$. Notably, Liu et al. (2019b)

Method	boston	concrete	energy	kin8nm	power	yacht	year	protein
LD	-2.52 (0.15)	-3.16 (0.04)	-2.36 (0.06)	0.10 (0.03)	-2.85 (0.03)	-1.60 (0.08)	-3.69 (0.01)	-3.05 (0.01)
SVGD	-2.60 (0.46)	-3.11 (0.10)	-1.95 (0.07)	1.03 (0.25)	-2.82 (0.03)	-1.66 (0.17)	-3.61 (0.00)	-2.91 (0.01)
Blob	-2.52 (0.32)	-3.19 (0.07)	-1.67 (0.03)	0.95 (0.03)	-2.81 (0.04)	-1.34 (0.07)	-3.60 (0.00)	-2.93 (0.01)
SGHMC-Blob	-2.42 (0.12)	-2.95 (0.01)	-1.36 (0.26)	1.23 (0.02)	-2.77 (0.04)	-0.73 (0.46)	-3.60 (0.02)	-3.73 (0.16)
SGNHT	-2.59 (0.13)	-3.41 (0.05)	-2.44 (0.04)	0.75 (0.02)	-2.86 (0.02)	-2.64 (0.04)	-3.69 (0.00)	-3.01 (0.01)
DE	-2.68 (0.63)	-2.96 (0.15)	-0.45 (0.14)	1.16 (0.02)	-2.80 (0.03)	-1.04 (0.40)	-3.68 (0.00)	-3.00 (0.01)
SGHMC-Stein	-2.81 (0.71)	-3.04 (0.25)	-1.40 (0.82)	1.25 (0.02)	-2.76 (0.04)	-0.86 (0.33)	-3.59 (0.00)	-2.90 (0.01)
SGNHT-Stein	-2.49 (0.30)	-2.97 (0.11)	-0.44 (0.10)	1.24 (0.03)	-2.78 (0.04)	-0.85 (0.21)	-3.59 (0.00)	-2.85 (0.01)

Table 2: The test log-likelihood (higher is better) results for selected datasets in UCI repository. The results are reported in mean (standard deviation) form averaged over 20 runs in the first 6 columns and 6 runs in the last 2, with the best performing model marked in boldface.

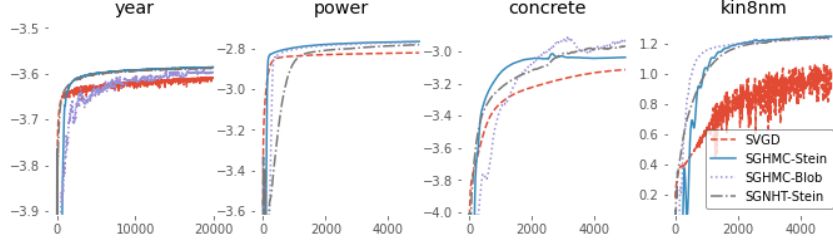


Figure 5: The trace plots of test log-likelihoods of BNN experiments: the x-axis determines the iterations. The figures show the effect of the momentum variables in SGHMC-Stein and SGNHT-Stein in exploring the posterior space, and quickly converging to better optima. The jaggedness of SVGD showcases that while SVGD empirically works with stochastic gradient, it is less robust with stochastic gradient noise.

propose an alternative vector field $\tilde{\mathbf{v}}^{\mathbf{A},\mathbf{C}}(\rho) = \mathbf{v}^{\mathbf{A},\mathbf{C}}(\rho) - \mathbf{C}\nabla \log \rho + \nabla \cdot \mathbf{C}$ ¹. A projection onto RKHS yields a Stein PARVI with update

$$\dot{\boldsymbol{\theta}}_t = \mathbb{E}_{\rho_t} \left[\frac{1}{\pi} \nabla \cdot [\pi(\mathbf{A} + \mathbf{C})] k(\boldsymbol{\theta}_t, \cdot) + \mathbf{A} \nabla_2 k(\boldsymbol{\theta}_t, \cdot) \right], \quad (24)$$

consistent with the standard formulation infinitesimal generator. However, the expectation in (24) notably does not converge to zero when $\rho_t = \pi$ (Gorham et al., 2019), suggesting that the particles will keep rotating along the trajectories of a divergence-free vector field, as opposed to stopping, in the equilibrium state. Interested readers can find experiments with respect to this alternative form in the supplementary materials.

5.2 Generalizing LAWGD with the diffusion Stein operator

The application of the diffusion Stein operator generalizes Laplacian Adjusted Wasserstein Gradient Descent (LAWGD) (Chewi et al., 2020), which views SVGD as a kernelized Wasserstein gradient flow driven by the chi-squared divergence. Given the first variation of the chi-squared divergence $\frac{\delta \chi^2[\rho \parallel \pi]}{\delta \rho} = \frac{2\rho}{\pi}$, we can verify that the vector field $\mathbf{v}_{\mathcal{H}}^{\mathbf{A},\mathbf{C}} = \mathcal{K}_{\rho} \left[(\mathbf{A} + \mathbf{C}) \nabla \log \frac{\rho}{\pi} \right]$ is rewritten as

$$2\mathbf{v}_{\mathcal{H}}^{\mathbf{A},\mathbf{C}} = \mathcal{K}_{\pi} \left[(\mathbf{A} + \mathbf{C}) \nabla \frac{2\rho}{\rho} \right] = \mathcal{K}_{\pi} \left[(\mathbf{A} + \mathbf{C}) \nabla \frac{\delta \chi^2[\rho_t \parallel \pi]}{\delta \rho_t} \right]. \quad (25)$$

The chi-squared divergence perspectives enriches GSVG as a kernelized fiber-gradient Hamiltonian flow minimizing the chi-squared divergence. Replacing the vector field $\mathcal{K}_{\pi} \left[(\mathbf{A} + \mathbf{C}) \nabla \frac{d\rho}{d\pi} \right]$ with $\mathbf{u} = \nabla \cdot \left(\mathcal{K}_{\pi} \left[(\mathbf{A} + \mathbf{C}) \frac{d\rho}{d\pi} \right] \right)$, we get the dissipation formula for the KL-divergence

$$\frac{d\text{KL}[\rho_t \parallel \pi]}{dt} = -\mathbb{E}_{\pi} \left\langle \nabla \cdot \frac{\rho}{\pi}, \nabla \cdot \left(\mathcal{K}_{\pi} \left[(\mathbf{A} + \mathbf{C}) \frac{\rho}{\pi} \right] \right) \right\rangle = -\mathbb{E}_{\pi} \left[\frac{\rho}{\pi} \mathcal{A}_{\pi}^{\mathbf{A},\mathbf{C}} \mathcal{K}_{\pi} \frac{\rho}{\pi} \right], \quad (26)$$

where $\mathcal{A}_{\pi}^{\mathbf{A},\mathbf{C}}$ represents the infinitesimal generator that induces the diffusion Stein operator: $\mathcal{A}_{\pi}^{\mathbf{A},\mathbf{C}} g = \frac{1}{2\pi} \nabla \cdot (\pi(\mathbf{A} + \mathbf{C})\nabla g)$. Following the construction of LAWGD, we choose the kernel so that $\mathcal{K}_{\pi} = (\mathcal{A}_{\pi}^{\mathbf{A},\mathbf{C}})^{-1}$. While it remains to be seen what kernel induces this equality, the diffusion Stein operator yields a more flexible formulation, while retaining the superior convergence of LAWGD.

6 Conclusion

We further the application of the Stein operator and its generalizations by proposing GSVG, an interacting particle system transporting a particle set towards a target distribution π in an emulation of the corresponding MCMC dynamics. We showcase theoretically and empirically that GSVG helps augment the well-researched field of efficient MCMC dynamics with deterministic interacting particle systems with high-quality samples.

¹In fact, a divergence-free vector field $\mathbf{C}_0 \nabla \log \rho - \nabla \cdot \mathbf{C}_0$ can be constructed out of an arbitrary skew-symmetric matrix-valued function \mathbf{C}_0

References

- Tianqi Chen, Emily Fox, and Carlos Guestrin. Stochastic gradient Hamiltonian Monte Carlo. In *International conference on machine learning*, pages 1683–1691, 2014.
- Yi-An Ma, Tianqi Chen, and Emily B. Fox. A complete recipe for stochastic gradient MCMC. In *NIPS’15 Proceedings of the 28th International Conference on Neural Information Processing Systems - Volume 2*, volume 28, pages 2917–2925, 2015.
- Qiang Liu and Dilin Wang. Stein variational gradient descent: A general purpose Bayesian inference algorithm. In *Advances in Neural Information Processing Systems*, volume 29, pages 2378–2386, 2016.
- Changyou Chen, Ruiyi Zhang, Wenlin Wang, Bai Li, and Liqun Chen. A unified particle-optimization framework for scalable Bayesian sampling. In *UAI*, pages 746–755, 2018.
- Chang Liu, Jingwei Zhuo, Pengyu Cheng, Ruiyi Zhang, and Jun Zhu. Understanding and accelerating particle-based variational inference. In *International Conference on Machine Learning*, pages 4082–4092, 2019a.
- Richard Jordan, David Kinderlehrer, and Felix Otto. The variational formulation of the Fokker-Planck equation. *SIAM Journal on Mathematical Analysis*, 29(1):1–17, 1998.
- Qiang Liu. Stein variational gradient descent as gradient flow. In *Advances in Neural Information Processing Systems*, volume 30, pages 3115–3123, 2017.
- Chang Liu, Jingwei Zhuo, and Jun Zhu. Understanding MCMC dynamics as flows on the Wasserstein space. In *International Conference on Machine Learning*, pages 4093–4103, 2019b.
- A. Duncan, N. Nuesken, and L. Szpruch. On the geometry of Stein variational gradient descent. *arXiv preprint arXiv:1912.00894*, 2019.
- Mark Girolami and Ben Calderhead. Riemann manifold langevin and hamiltonian monte carlo methods. *Journal of The Royal Statistical Society Series B-statistical Methodology*, 73(2):123–214, 2011.
- Max Welling and Yee W. Teh. Bayesian learning via stochastic gradient Langevin dynamics. In *Proceedings of the 28th International Conference on Machine Learning*, pages 681–688, 2011.
- Chang Liu and Jun Zhu. Riemannian Stein variational gradient descent for bayesian inference. In *AAAI*, pages 3627–3634, 2017.
- P. Langevin. Sur la theorie du mouvement Brownien. *Compt. Rendus*, 146:530–533, 1908.
- Hannes Risken. Fokker-Planck equation. pages 63–95, 1996.
- Lars Onsager. Reciprocal relations in irreversible processes. ii. *Physical Review*, 37(12):2265–2279, 1931.
- José Antonio Carrillo, Katy Craig, and Francesco S. Patacchini. A blob method for diffusion. *Calculus of Variations and Partial Differential Equations*, 58(2):1–53, 2019.
- Charles Stein. A bound for the error in the normal approximation to the distribution of a sum of dependent random variables. *Proceedings of the Sixth Berkeley Symposium on Mathematical Statistics and Probability, Volume 2: Probability Theory*, 1972.
- Jackson Gorham, Andrew B. Duncan, Sebastian J. Vollmer, and Lester Mackey. Measuring sample quality with diffusions. *Annals of Applied Probability*, 29(5):2884–2928, 2019.
- A. D. Barbour. Stein’s method and Poisson process convergence. *Journal of Applied Probability*, 25: 175–184, 1988.
- A. D. Barbour. Stein’s method for diffusion approximations. *Probability Theory and Related Fields*, 84(3):297–322, 1990.

- F. Gotze. On the rate of convergence in the multivariate CLT. *Annals of Probability*, 19(2):724–739, 1991.
- Alessandro Barp, François-Xavier Briol, Andrew B. Duncan, Mark A. Girolami, and Lester W. Mackey. Minimum stein discrepancy estimators. In *Advances in Neural Information Processing Systems*, volume 32, pages 12964–12976, 2019.
- Jianyi Zhang, Ruiyi Zhang, Lawrence Carin, and Changyou Chen. Stochastic particle-optimization sampling and the non-asymptotic convergence theory. In *International Conference on Artificial Intelligence and Statistics*, pages 1877–1887, 2020.
- Yingzhen Li and Richard E. Turner. Gradient estimators for implicit models. In *International Conference on Learning Representations*, 2017.
- Yi-An Ma, Niladri S. Chatterji, Xiang Cheng, Nicolas Flammarion, Peter L. Bartlett, and Michael I. Jordan. Is there an analog of Nesterov acceleration for MCMC. *arXiv preprint arXiv:1902.00996*, 2019.
- Yifei Wang and Wuchen Li. Accelerated information gradient flow. *arXiv preprint arXiv:1909.02102*, 2019.
- Nan Ding, Youhan Fang, Ryan Babbush, Changyou Chen, Robert D Skeel, and Hartmut Neven. Bayesian sampling using stochastic gradient thermostats. In *Advances in Neural Information Processing Systems 27*, volume 27, pages 3203–3211, 2014.
- Sinho Chewi, Thibaut Le Gouic, Chen Lu, Tyler Maunu, and Philippe Rigollet. SVGD as a kernelized Wasserstein gradient flow of the chi-squared divergence. In *Advances in Neural Information Processing Systems*, volume 33, pages 2098–2109, 2020.

Supplementary material to De-randomizing MCMC dynamics with the generalized Stein operator

Zheyang Shen Markus Heinonen Samuel Kaski
Department of Computer Science
Aalto University, Finland
first.last@aalto.fi

In the supplementary material, we expand on the background details and derivations mentioned in the paper.

1 Additional derivations for the Wasserstein gradient flow

1.1 Stochastic differential equations and its Fokker-Planck equation

The general SDE

$$d\boldsymbol{\theta}_t = \underbrace{\mathbf{f}(\boldsymbol{\theta}_t)}_{\text{drift}} dt + \underbrace{\sqrt{2\Sigma(\boldsymbol{\theta}_t)}}_{\text{diffusion}} \underbrace{d\mathbf{W}_t}_{\text{Wiener process}} \quad (1)$$

with an initial distribution $\boldsymbol{\theta}_0 \sim \rho_0$ defines the evolution of a random variable $\boldsymbol{\theta}_t \in \mathbb{R}^D$ over time $t \in \mathbb{R}_+$. The evolution of the marginal distribution ρ_t is given by the Fokker-Planck equation

$$\dot{\rho}_t(\boldsymbol{\theta}) = - \sum_{i=1}^D \frac{\partial}{\partial \theta_i} \rho_t(\boldsymbol{\theta}) f_i(\boldsymbol{\theta}) + \sum_{i,j=1}^D \frac{\partial^2}{\partial \theta_i \partial \theta_j} \rho_t(\boldsymbol{\theta}) \Sigma_{ij}(\boldsymbol{\theta}) \quad (2)$$

$$= -\nabla \cdot (\rho_t \mathbf{f}) + (\nabla^\top \nabla) : (\rho_t \boldsymbol{\Sigma}), \quad (3)$$

where we use the dyadic vector notation

$$\mathbf{A} : \mathbf{B} = \text{tr}\{\mathbf{A}^\top \mathbf{B}\}. \quad (4)$$

The double-dot notation indicates a sum over all element-wise products, or the sum of all second order partial derivatives. We can verify this with

$$(\nabla^\top \nabla) : (\rho_t \boldsymbol{\Sigma}) = \text{tr}\{(\nabla^\top \nabla)^\top (\rho_t \boldsymbol{\Sigma})\} \quad (5)$$

$$= \text{tr}\{(\nabla \nabla^\top)(\rho_t \boldsymbol{\Sigma})\} \quad (6)$$

$$= \langle \nabla \nabla^\top, \rho_t \boldsymbol{\Sigma} \rangle_F \quad (7)$$

$$= \sum_{i,j} \frac{\partial^2}{\partial \theta_i \partial \theta_j} \rho_t(\boldsymbol{\theta}_t) \Sigma_{ij}(\boldsymbol{\theta}_t). \quad (8)$$

1.2 FPE of Langevin dynamics

The Langevin dynamics has drift $\mathbf{f}(\boldsymbol{\theta}_t) = \nabla \log \pi(\boldsymbol{\theta}_t)$ and diffusion $\Sigma(\boldsymbol{\theta}_t) = \mathbf{I}$. The Fokker-Planck equation for Langevin dynamics then simplifies into

$$\dot{\rho}_t = -\nabla \cdot (\rho_t \mathbf{f}) + (\nabla \nabla^\top) : (\rho_t \mathbf{I}) \quad (9)$$

$$= -\nabla \cdot (\rho_t \nabla \log \pi) + \Delta \rho_t, \quad (10)$$

where the Laplacian is defined as

$$\Delta \rho_t = \nabla^2 \rho_t = \sum_{i=1}^D \frac{\partial^2 \rho_t(\boldsymbol{\theta})}{\partial \theta_i^2}. \quad (11)$$

To derive the FPE we begin by using the Laplacian identity $\Delta \rho_t = \nabla \cdot (\nabla \rho_t)$, resulting in

$$\dot{\rho}_t = \Delta \rho_t - \nabla \cdot (\rho_t \nabla \log \pi) \quad (12)$$

$$= \nabla \cdot (\nabla \rho_t) - \nabla \cdot (\rho_t \nabla \log \pi) \quad (13)$$

$$= \nabla \cdot (\nabla \rho_t - \rho_t \nabla \log \pi) \quad (14)$$

$$= \nabla \cdot (\rho_t \nabla \log \rho_t - \rho_t \nabla \log \pi) \quad (15)$$

$$= \nabla \cdot \left(\rho_t \nabla \log \frac{\rho_t}{\pi} \right), \quad (16)$$

where we used the identity $\nabla \log \rho = \frac{\nabla \rho}{\rho}$ to expand $\nabla \rho = \rho \nabla \log \rho$. Notice that we did not need to use the common identity $\nabla \cdot (\rho \mathbf{f}) = \rho \nabla \cdot \mathbf{f} + (\nabla \rho) \cdot \mathbf{f}$, nor expand with $\nabla \log \pi = -\nabla H$.

We also notice that the first variation of the Kullback-Leibler divergence has the form $\frac{\delta \text{KL}[\rho_t \parallel \pi]}{\delta \rho_t} = \log \rho_t / \pi + 1$, so that $\nabla \frac{\delta \text{KL}[\rho_t \parallel \pi]}{\delta \rho_t} = \nabla \log \rho_t - \nabla \log \pi$, yielding the final result

$$\dot{\rho}_t = \nabla \cdot \left(\rho_t \nabla \frac{\delta \text{KL}[\rho_t \parallel \pi]}{\delta \rho_t} \right). \quad (17)$$

In the original variational formulation for the Wasserstein gradient flow (Jordan et al., 1998), the authors prove the weak convergence of a discrete gradient flow taking discrete steps at interval h , such that each $\rho_{kh}, k = 1, 2, \dots$, follows the minimization

$$\rho_{kh} = \arg \min_{\rho \in \mathcal{P}(\Omega)} \text{KL}[\rho \parallel \pi] + \frac{1}{2h} W_2^2(\rho, \rho_{(k-1)h}). \quad (18)$$

$(\rho_{kh})_{k=1}^\infty$ weakly converges to the Fokker-Planck equation as $h \downarrow 0$.

1.3 The Stein-Wasserstein metric

With the Onsager operator defined as $G(\rho)^{-1} : \phi \mapsto -\nabla \cdot (\rho \mathcal{K}_\rho \nabla \phi)$, the Stein-Wasserstein metric between ρ_0 and ρ_1 is defined using the geometric action function

$$W_{\mathcal{H}}^2(\rho_0, \rho_1) = \inf_{\phi, \rho_t} \left\{ \int_0^1 \int \|\mathcal{K}_{\rho_t} \nabla \phi_t\|_{\mathcal{H}}^2 dt : \dot{\rho}_t + \nabla \cdot (\rho_t \mathcal{K}_{\rho_t} \nabla \phi_t) = 0 \right\}, \quad (19)$$

where \mathcal{K}_ρ is the integral operator

$$\mathcal{K}_\rho \mathbf{f}(\boldsymbol{\theta}) = \int k(\boldsymbol{\theta}', \boldsymbol{\theta}) \mathbf{f}(\boldsymbol{\theta}') d\rho(\boldsymbol{\theta}'), \quad (20)$$

which smoothens the function \mathbf{f} over a similar parameters $\boldsymbol{\theta}'$ from the density ρ according to the kernel $k(\boldsymbol{\theta}', \boldsymbol{\theta})$. The Stein-Wasserstein metric follows the definition that the distance between two points in $\mathcal{P}(\Omega)$ consists of the length the shortest arc connecting the two points, parametrized by ϕ_t .

2 Additional derivations for the analysis of MCMC dynamics

To recap, MCMC dynamics consist of positive semi-definite matrix-valued function \mathbf{A} and skew-symmetric matrix-valued function \mathbf{C} with

$$\mathbf{f}(\boldsymbol{\theta}) = \frac{1}{\pi(\boldsymbol{\theta})} \nabla \cdot (\pi(\boldsymbol{\theta})(\mathbf{A}(\boldsymbol{\theta}) + \mathbf{C}(\boldsymbol{\theta}))), \quad (21)$$

$$\boldsymbol{\Sigma}(\boldsymbol{\theta}) = \mathbf{A}(\boldsymbol{\theta}) \quad (22)$$

with matrix properties

$$\mathbf{x}^\top \mathbf{A} \mathbf{x} \geq 0, \quad \forall \mathbf{x} \in \mathbb{R}^D \quad (23)$$

$$\mathbf{C}^\top = -\mathbf{C}, \quad C_{ij} = -C_{ji}, \quad \text{diag } \mathbf{C} = \mathbf{0}. \quad (24)$$

2.1 Fokker-Planck equation and its equivalent forms

We derive the Fokker-Planck equation of SDEs with the above MCMC dynamics form as

$$\dot{\rho}_t(\boldsymbol{\theta}) = -\sum_{i=1}^D \frac{\partial}{\partial \theta_i} \rho_t(\boldsymbol{\theta}) f_i(\boldsymbol{\theta}) + \sum_{i,j=1}^D \frac{\partial^2}{\partial \theta_i \partial \theta_j} \rho_t(\boldsymbol{\theta}) A_{ij}(\boldsymbol{\theta}) \quad (25)$$

$$= -\sum_{i=1}^D \frac{\partial}{\partial \theta_i} \rho_t(\boldsymbol{\theta}) f_i(\boldsymbol{\theta}) + \sum_{i,j=1}^D \frac{\partial^2}{\partial \theta_i \partial \theta_j} \rho_t(\boldsymbol{\theta}) A_{ij}(\boldsymbol{\theta}) + \underbrace{\sum_{i,j=1}^D \frac{\partial^2}{\partial \theta_i \partial \theta_j} \rho_t(\boldsymbol{\theta}) C_{ij}(\boldsymbol{\theta})}_{=0} \quad (26)$$

$$= -\nabla \cdot \left(\frac{\rho_t}{\pi} \nabla \cdot (\pi(\mathbf{A} + \mathbf{C})) \right) + (\nabla^\top \nabla) : (\rho_t(\mathbf{A} + \mathbf{C})) \quad (27)$$

$$= -\nabla \cdot (\rho_t [(\mathbf{A} + \mathbf{C}) \nabla \log \pi(\boldsymbol{\theta}) + \nabla \cdot (\mathbf{A} + \mathbf{C})]) + (\nabla^\top \nabla) : (\rho_t(\mathbf{A} + \mathbf{C})) \quad (28)$$

$$= -\nabla \cdot (\rho_t [(\mathbf{A} + \mathbf{C}) \nabla \log \pi(\boldsymbol{\theta}) + \nabla \cdot (\mathbf{A} + \mathbf{C})]) + \nabla \cdot (\rho_t [(\mathbf{A} + \mathbf{C}) \nabla \log \rho_t + \nabla \cdot (\mathbf{A} + \mathbf{C})]) \quad (29)$$

$$= \nabla \cdot \left(\rho_t(\mathbf{A} + \mathbf{C}) \nabla \log \frac{\rho_t}{\pi} \right), \quad (30)$$

where the skew-symmetric addition is justified via

$$\sum_{i,j=1}^D \frac{\partial^2}{\partial \theta_i \partial \theta_j} \rho_t(\boldsymbol{\theta}) C_{ij}(\boldsymbol{\theta}) = \underbrace{\sum_{i,j=1}^D \frac{\partial^2 \rho_t(\boldsymbol{\theta})}{\partial \theta_i \partial \theta_j} C_{ij}(\boldsymbol{\theta})}_{=0} + \underbrace{\sum_{i,j=1}^D \rho_t(\boldsymbol{\theta}) \frac{\partial^2 C_{ij}(\boldsymbol{\theta})}{\partial \theta_i \partial \theta_j}}_{=0} \quad (31)$$

$$+ \sum_{i,j=1}^D \left[\frac{\partial \rho_t(\boldsymbol{\theta})}{\partial \theta_i} \frac{\partial C_{ij}(\boldsymbol{\theta})}{\partial \theta_j} + \frac{\partial \rho_t(\boldsymbol{\theta})}{\partial \theta_j} \frac{\partial C_{ij}(\boldsymbol{\theta})}{\partial \theta_i} \right] \quad (32)$$

$$= \sum_{i,j=1}^D \frac{\partial \rho_t(\boldsymbol{\theta})}{\partial \theta_i} \frac{\partial C_{ij}(\boldsymbol{\theta})}{\partial \theta_j} + \sum_{j,i=1}^D \frac{\partial \rho_t(\boldsymbol{\theta})}{\partial \theta_j} \frac{\partial C_{ij}(\boldsymbol{\theta})}{\partial \theta_i} \quad (33)$$

$$= \sum_{i,j=1}^D \frac{\partial \rho_t(\boldsymbol{\theta})}{\partial \theta_i} \frac{\partial C_{ij}(\boldsymbol{\theta})}{\partial \theta_j} + \sum_{j,i=1}^D \frac{\partial \rho_t(\boldsymbol{\theta})}{\partial \theta_j} \frac{\partial -C_{ji}(\boldsymbol{\theta})}{\partial \theta_i} = 0. \quad (34)$$

The final form (30) corresponds to a generalization of the continuity equation $\dot{\rho}_t + \nabla \cdot (\rho_t(\mathbf{A} + \mathbf{C}) \nabla \phi_t) = 0$.

2.2 The diffusion Stein operator

Originally, the Stein's identity (Stein, 1972) maps sufficiently regular functions $\Phi : \mathbb{R}^D \mapsto \mathbb{R}^D$ to $\mathcal{T}\Phi(\boldsymbol{\theta}) = \nabla \log \pi(\boldsymbol{\theta}) \cdot \Phi(\boldsymbol{\theta}) + \nabla \cdot \Phi(\boldsymbol{\theta})$. The function $\mathcal{T}\Phi$ has expectation zero under the target measure π : $\mathbb{E}_\pi \mathcal{T}\Phi = 0$, yielding the original Stein's identity. As a generalization, Gorham et al. (2019) discuss the application of infinitesimal generator of MCMC dynamics as a means to discover operators sharing the same property. Infinitesimal generators of Feller processes describes the perturbation of functions:

$$\mathcal{A}u(\boldsymbol{\theta}) = \lim_{t \rightarrow 0} \frac{\mathbb{E}[u(\boldsymbol{\theta}_t) | \boldsymbol{\theta}_0 = \boldsymbol{\theta}] - u(\boldsymbol{\theta})}{t}. \quad (35)$$

For MCMC dynamics with parametrization (\mathbf{A}, \mathbf{C}) , the infinitesimal generator is calculated as

$$(\mathcal{A}_\pi^{\mathbf{A}, \mathbf{C}} u)(\boldsymbol{\theta}) = \frac{1}{2\pi(\boldsymbol{\theta})} \nabla \cdot (\pi(\boldsymbol{\theta})(\mathbf{A}(\boldsymbol{\theta}) + \mathbf{C}(\boldsymbol{\theta})) \nabla u(\boldsymbol{\theta})). \quad (36)$$

And the *diffusion Stein operator*, denoted as $\mathcal{T}_\pi^{\mathbf{A}, \mathbf{C}}$ in this work, is defined by substituting $\frac{\nabla u}{2}$ with a vector-valued function \mathbf{f} . GSVG is defined as $\mathbb{E}_\rho \mathcal{T}_\pi^{\mathbf{A}, \mathbf{C}} k(\cdot, \boldsymbol{\theta})$.

2.3 GSVG as functional gradient in RKHS for incremental transformations

Functional gradient for a functional $F[\cdot]$ is defined as such $\nabla_{\mathbf{f}} F[\mathbf{f}]$ that satisfies $F[\mathbf{f} + \epsilon \mathbf{g}] = F[\mathbf{f}] + \langle \nabla_{\mathbf{f}} F[\mathbf{f}], \mathbf{g} \rangle_{\mathcal{H}^D} + O(\epsilon^2)$. The particle update of GSVG can be seen as the functional gradient with respect to the push-forward measure $\rho_\epsilon = (\text{id} + (\mathbf{A} + \mathbf{C})^\top \mathbf{f})_{\#} \rho = (\text{id} + (\mathbf{A} - \mathbf{C})\mathbf{f})_{\#} \rho$. Following the proof of Theorem 3.3 in [Liu and Wang \(2016\)](#), we define $F[\mathbf{f}] = \text{KL}[\rho_\epsilon \parallel \pi] = \text{KL}[(\text{id} + (\mathbf{A} - \mathbf{C})\mathbf{f})_{\#} \rho \parallel \pi] = \text{KL}[\rho \parallel (\text{id} + (\mathbf{A} - \mathbf{C})\mathbf{f})_{\#}^{-1} \pi]$

$$F[\mathbf{f} + \epsilon \mathbf{g}] = \mathbb{E}_\rho \left[\log \rho(\boldsymbol{\theta}) - \log \pi(\boldsymbol{\theta} + (\mathbf{A} - \mathbf{C})(\mathbf{f} + \epsilon \mathbf{g})) - \log \det \left(\mathbf{I} + \underbrace{\nabla((\mathbf{A} - \mathbf{C})(\mathbf{f} + \epsilon \mathbf{g}))}_{\text{Jacobian matrix}} \right) \right]. \quad (37)$$

We then have

$$F[\mathbf{f} + \epsilon \mathbf{g}] - F[\mathbf{f}] = - \underbrace{\mathbb{E}_\rho \left[\log \frac{\pi(\boldsymbol{\theta} + (\mathbf{A} - \mathbf{C})(\mathbf{f} + \epsilon \mathbf{g}))}{\pi(\boldsymbol{\theta} + (\mathbf{A} - \mathbf{C})\mathbf{f})} \right]}_{\Delta_1} - \underbrace{\mathbb{E}_\rho \left[\log \frac{\det(\mathbf{I} + \nabla((\mathbf{A} - \mathbf{C})(\mathbf{f} + \epsilon \mathbf{g})))}{\det(\mathbf{I} + \nabla((\mathbf{A} - \mathbf{C})\mathbf{f}))} \right]}_{\Delta_2}. \quad (38)$$

$$\Delta_1 = \mathbb{E}_\rho [\log \pi(\boldsymbol{\theta} + (\mathbf{A} - \mathbf{C})(\mathbf{f} + \epsilon \mathbf{g})) - \log \pi(\boldsymbol{\theta} + (\mathbf{A} - \mathbf{C})\mathbf{f})] \quad (39)$$

$$= \epsilon \mathbb{E}_\rho [\nabla \log \pi(\boldsymbol{\theta} + (\mathbf{A} - \mathbf{C})\mathbf{f}) \cdot (\mathbf{A} - \mathbf{C})\mathbf{g}] + O(\epsilon^2) \quad (40)$$

$$= \mathbb{E}_\rho [(\mathbf{A} + \mathbf{C})\nabla \log \pi(\boldsymbol{\theta} + (\mathbf{A}(\boldsymbol{\theta}) - \mathbf{C}(\boldsymbol{\theta}))\mathbf{f}(\boldsymbol{\theta})))] \cdot \mathbf{g} + O(\epsilon^2) \quad (41)$$

$$= \mathbb{E}_{\boldsymbol{\theta} \sim \rho} [(\mathbf{A}(\boldsymbol{\theta}) + \mathbf{C}(\boldsymbol{\theta}))\nabla \log \pi(\boldsymbol{\theta} + (\mathbf{A}(\boldsymbol{\theta}) - \mathbf{C}(\boldsymbol{\theta}))\mathbf{f}(\boldsymbol{\theta})))] \cdot \langle k(\boldsymbol{\theta}, \cdot), \mathbf{g}(\cdot) \rangle_{\mathcal{H}^D} + O(\epsilon^2) \quad (42)$$

$$= \langle \mathbb{E}_{\boldsymbol{\theta} \sim \rho} [(\mathbf{A}(\boldsymbol{\theta}) + \mathbf{C}(\boldsymbol{\theta}))\nabla \log \pi(\boldsymbol{\theta} + (\mathbf{A}(\boldsymbol{\theta}) - \mathbf{C}(\boldsymbol{\theta}))\mathbf{f}(\boldsymbol{\theta})))] k(\boldsymbol{\theta}, \cdot), \mathbf{g}(\cdot) \rangle_{\mathcal{H}^D} + O(\epsilon^2), \quad (43)$$

$$\Delta_2 = \mathbb{E}_\rho [\log \det(\mathbf{I} + \nabla((\mathbf{A} - \mathbf{C})(\mathbf{f} + \epsilon \mathbf{g}))) - \log \det(\mathbf{I} + \nabla((\mathbf{A} - \mathbf{C})\mathbf{f}))] \quad (44)$$

$$= \epsilon \mathbb{E}_\rho \left[(\mathbf{I} + \nabla((\mathbf{A} - \mathbf{C})\mathbf{f}))^{-1} : \nabla((\mathbf{A} - \mathbf{C})\mathbf{g}) \right] + O(\epsilon^2) \quad (45)$$

$$= \epsilon \mathbb{E}_\rho \left[(\mathbf{I} + \nabla((\mathbf{A} - \mathbf{C})\mathbf{f}))^{-1} : \left\{ \underbrace{(\mathbf{A} - \mathbf{C})\nabla \mathbf{g}}_{\Delta_3} + \underbrace{\mathbf{M}}_{\Delta_4} \right\} \right] + O(\epsilon^2), \quad (46)$$

where $\mathbf{M}_{ij} = \sum_{\ell=1}^D \frac{\partial(\mathbf{A}-\mathbf{C})_{i\ell}}{\partial \theta_j} g_\ell$. We have

$$\mathbf{M}_{ij}(\boldsymbol{\theta}) = \sum_{\ell=1}^D \frac{\partial(\mathbf{A}(\boldsymbol{\theta}) - \mathbf{C}(\boldsymbol{\theta}))_{i\ell}}{\partial \theta_j} g_\ell(\boldsymbol{\theta}) \quad (47)$$

$$= \sum_{\ell=1}^D \frac{\partial(\mathbf{A}(\boldsymbol{\theta}) - \mathbf{C}(\boldsymbol{\theta}))_{i\ell}}{\partial \theta_j} \langle k(\boldsymbol{\theta}, \cdot), g_\ell(\cdot) \rangle_{\mathcal{H}} \quad (48)$$

$$= \langle \mathbf{h}^{(ij)} k(\boldsymbol{\theta}, \cdot), \mathbf{g}(\cdot) \rangle_{\mathcal{H}^D}, \quad (49)$$

where $\mathbf{h}_\ell^{(ij)} = \frac{\partial(\mathbf{A}(\boldsymbol{\theta}) - \mathbf{C}(\boldsymbol{\theta}))_{i\ell}}{\partial\theta_j}$.

$$\Delta_3 = \epsilon \mathbb{E}_\rho \left[(\mathbf{I} + \nabla((\mathbf{A} - \mathbf{C})\mathbf{f}))^{-1} : \{(\mathbf{A} - \mathbf{C}) \nabla \mathbf{g}\} \right] \quad (50)$$

$$= \epsilon \mathbb{E}_\rho \left[(\mathbf{I} + \nabla((\mathbf{A} - \mathbf{C})\mathbf{f}))^{-1} (\mathbf{A} + \mathbf{C}) : \nabla \mathbf{g} \right] \quad (51)$$

$$= \epsilon \mathbb{E}_{\boldsymbol{\theta} \sim \rho} \left[(\mathbf{I} + \nabla((\mathbf{A}(\boldsymbol{\theta}) - \mathbf{C}(\boldsymbol{\theta}))\mathbf{f}(\boldsymbol{\theta})))^{-1} (\mathbf{A}(\boldsymbol{\theta}) + \mathbf{C}(\boldsymbol{\theta})) : \langle \nabla_1 k(\boldsymbol{\theta}, \cdot), \mathbf{g}(\cdot) \rangle_{\mathcal{H}^D} \right] \quad (52)$$

$$= \epsilon \left\langle \mathbb{E}_{\boldsymbol{\theta} \sim \rho} \left[(\mathbf{I} + \nabla((\mathbf{A}(\boldsymbol{\theta}) - \mathbf{C}(\boldsymbol{\theta}))\mathbf{f}(\boldsymbol{\theta})))^{-1} (\mathbf{A}(\boldsymbol{\theta}) + \mathbf{C}(\boldsymbol{\theta})) \nabla_1 k(\boldsymbol{\theta}, \cdot), \mathbf{g}(\cdot) \right] \right\rangle_{\mathcal{H}^D}, \quad (53)$$

$$\Delta_4 = \epsilon \mathbb{E}_{\boldsymbol{\theta} \sim \rho} \left[\underbrace{(\mathbf{I} + \nabla((\mathbf{A}(\boldsymbol{\theta}) - \mathbf{C}(\boldsymbol{\theta}))\mathbf{f}(\boldsymbol{\theta})))^{-1}}_{\mathbf{Q}(\boldsymbol{\theta})} : \mathbf{M} \right] \quad (54)$$

$$= \epsilon \mathbb{E}_{\boldsymbol{\theta} \sim \rho} \sum_{i,j=1}^D \mathbf{Q}_{ij} \mathbf{M}_{ij} = \epsilon \left\langle \mathbb{E}_{\boldsymbol{\theta} \sim \rho} \sum_{i,j=1}^D \mathbf{Q}_{ij} \mathbf{h}^{(ij)} k(\boldsymbol{\theta}, \cdot), \mathbf{g}(\cdot) \right\rangle_{\mathcal{H}^D} \quad (55)$$

It is straightforward that when $\mathbf{f} = \mathbf{0}$,

$$\Delta_4 = \epsilon \mathbb{E}_{\boldsymbol{\theta} \sim \rho} \left\langle \sum_{i=1}^D \mathbf{h}^{(ii)} k(\boldsymbol{\theta}, \cdot), \mathbf{g} \right\rangle_{\mathcal{H}^D}, \quad (56)$$

$$\sum_{i=1}^D \mathbf{h}_\ell^{(ii)} = \sum_{i=1}^D \frac{\partial(\mathbf{A} - \mathbf{C})_{i\ell}}{\partial\theta_i} \quad (57)$$

$$= \sum_{i=1}^D \frac{\partial(\mathbf{A} + \mathbf{C})_{\ell i}}{\partial\theta_i} = \nabla \cdot (\mathbf{A} + \mathbf{C}). \quad (58)$$

Using the definition of $\Delta_i, i \in [4]$, we can derive the GSVGD particle update as $\mathbf{f} = \mathbf{0}$, confirming the functional derivative coinciding with the GSVGD particle update.

2.4 Projection onto RKHS

To prove $\mathbf{v}_{\mathcal{H}}^{\mathbf{A}, \mathbf{C}}$ is the projection of $\mathbf{v}^{\mathbf{A}, \mathbf{C}}$ onto \mathcal{H}^D , we start from the inner product on \mathcal{L}_ρ^2 , such that $\forall \mathbf{v} \in \mathcal{H}^D$

$$\langle \mathbf{v}^{\mathbf{A}, \mathbf{C}}(\cdot | \rho), \mathbf{v} \rangle_{\mathcal{L}_\rho^2} = \mathbb{E}_\rho [(\mathbf{A} + \mathbf{C}) \nabla \log \pi / \rho \cdot \mathbf{v}] \quad (59)$$

$$= \mathbb{E}_\rho [(\mathbf{A} + \mathbf{C}) \nabla \log \pi \cdot \mathbf{v}] - \mathbb{E}_\rho [(\mathbf{A} + \mathbf{C}) \nabla \log \rho \cdot \mathbf{v}] \quad (60)$$

$$= \mathbb{E}_\rho [(\mathbf{A} + \mathbf{C}) \nabla \log \pi \cdot \mathbf{v}] - \underbrace{\int [(\mathbf{A} + \mathbf{C}) \nabla \rho \cdot \mathbf{v}] d\boldsymbol{\theta}}_{\text{weak derivative of measures}} \quad (61)$$

$$= \mathbb{E}_\rho [(\mathbf{A} + \mathbf{C}) \nabla \log \pi \cdot \mathbf{v}] + \mathbb{E}_\rho \left[\sum_{i,j} \frac{\partial((\mathbf{A}_{ij} + \mathbf{C}_{ij})v_i)}{\partial\theta_j} \right] \quad (62)$$

$$= \mathbb{E}_\rho [\{(\mathbf{A} + \mathbf{C}) \nabla \log \pi + \nabla \cdot (\mathbf{A} + \mathbf{C})\} \cdot \mathbf{v}] + \mathbb{E}_\rho \left[\sum_{i,j} \frac{(\mathbf{A}_{ij} + \mathbf{C}_{ij}) \partial v_i}{\partial\theta_j} \right] \quad (63)$$

$$= \left\langle \mathbb{E}_{\boldsymbol{\theta} \sim \rho} \{(\mathbf{A}(\boldsymbol{\theta}) + \mathbf{C}(\boldsymbol{\theta})) \nabla \log \pi(\boldsymbol{\theta}) + \nabla \cdot (\mathbf{A}(\boldsymbol{\theta}) + \mathbf{C}(\boldsymbol{\theta}))\} k(\boldsymbol{\theta}, \cdot), \mathbf{v}(\cdot) \right\rangle_{\mathcal{H}^D} \quad (64)$$

$$+ \mathbb{E}_\rho \left[\sum_{i,j} \frac{(\mathbf{A}_{ij} + \mathbf{C}_{ij}) \partial v_i}{\partial\theta_j} \right], \quad (65)$$

$$\mathbb{E}_\rho \left[\sum_{i,j} \frac{(\mathbf{A}_{ij} + \mathbf{C}_{ij}) \partial v_i}{\partial \theta_j} \right] = \mathbb{E}_{\boldsymbol{\theta} \sim \rho} \left[\sum_{i,j} (\mathbf{A}_{ij}(\boldsymbol{\theta}) + \mathbf{C}_{ij}(\boldsymbol{\theta})) \frac{\partial v_i(\boldsymbol{\theta})}{\partial \theta_j} \right] \quad (66)$$

$$= \mathbb{E}_{\boldsymbol{\theta} \sim \rho} \left[\sum_{i,j} (\mathbf{A}_{ij}(\boldsymbol{\theta}) + \mathbf{C}_{ij}(\boldsymbol{\theta})) \left\langle \frac{\partial}{\partial \theta_j} k(\boldsymbol{\theta}, \cdot), \mathbf{v}_i(\cdot) \right\rangle_{\mathcal{H}} \right] \quad (67)$$

$$= \left\langle \mathbb{E}_{\boldsymbol{\theta} \sim \rho} [(\mathbf{A} + \mathbf{C}) \nabla k(\boldsymbol{\theta}, \cdot)], \mathbf{v}(\cdot) \right\rangle_{\mathcal{H}^D}. \quad (68)$$

Therefore, confirming that $\forall \mathbf{v} \in \mathcal{H}^D, \langle \mathbf{v}^{\mathbf{A}, \mathbf{C}}, \mathbf{v} \rangle_{\mathcal{L}_\rho^2} = \langle \mathbf{v}_{\mathcal{H}}^{\mathbf{A}, \mathbf{C}}, \mathbf{v} \rangle_{\mathcal{H}^D}$.

2.5 Interpreting GSVGD as MCMC dynamics of $\pi^{\otimes N}$

Additionally, we can view GSVGD with constant \mathbf{C} matrices and N particles as the mean-field limit of a MCMC dynamics inferring the product target measure $\underbrace{\pi \times \dots \times \pi}_N = \pi^{\otimes N}$, a rather trivial extension of the discussion in (Gallego and Insua, 2018). The $\mathbf{A}(\boldsymbol{\theta}^{\otimes N}), \mathbf{C}(\boldsymbol{\theta}^{\otimes N}) \in \mathbb{R}^{ND \times ND}$ is defined as

$$\tilde{\mathbf{A}}_{i,j} = \frac{1}{N} k(\boldsymbol{\theta}_i, \boldsymbol{\theta}_j) \frac{\mathbf{A}(\boldsymbol{\theta}_i) + \mathbf{A}(\boldsymbol{\theta}_j)}{2}, \quad (69)$$

$$\tilde{\mathbf{C}}_{i,j} = \frac{1}{N} k(\boldsymbol{\theta}_i, \boldsymbol{\theta}_j) \left[\mathbf{C} + \frac{\mathbf{A}(\boldsymbol{\theta}_j) - \mathbf{A}(\boldsymbol{\theta}_i)}{2} \right]. \quad (70)$$

We can verify that the MCMC dynamics

$$\dot{\boldsymbol{\theta}}_t^{\otimes N} = \frac{1}{\pi(\boldsymbol{\theta}^{\otimes N})} \nabla \cdot \left(\pi(\boldsymbol{\theta}_t^{\otimes N}) \left(\tilde{\mathbf{A}}(\boldsymbol{\theta}_t^{\otimes N}) + \tilde{\mathbf{C}}(\boldsymbol{\theta}_t^{\otimes N}) \right) \right) + \sqrt{2\tilde{\mathbf{A}}(\boldsymbol{\theta}_t^{\otimes N})} d\mathbf{W}_{ND}, \quad (71)$$

takes the invariant measure $\pi^{\otimes N}$. And that the drift coefficient corresponds to the GSVGD particle update. Furthermore, this framework accepts non-constant \mathbf{C} matrices when $\tilde{\mathbf{A}}_{i,j} = \frac{1}{N} k(\boldsymbol{\theta}_i, \boldsymbol{\theta}_j) \left[\frac{\mathbf{A}(\boldsymbol{\theta}_i) + \mathbf{A}(\boldsymbol{\theta}_j)}{2} + \frac{\mathbf{C}(\boldsymbol{\theta}_j) - \mathbf{C}(\boldsymbol{\theta}_i)}{2} \right]$ remains positive semidefinite.

It is worth noting that as $N \rightarrow \infty$, the drift coefficient goes to $\mathbf{0}$, making GSVGD the mean-field limit of such dynamics.

2.6 Stochastic particle optimization sampling (SPOS) as MCMC dynamics

Viewing GSVGD as the mean-field limit of MCMC dynamics yields additional insights. For example, Zhang et al. (2020) propose stochastic particle optimization sampling in the form of

$$\dot{\boldsymbol{\theta}}_t^{\otimes N} = \frac{1}{\pi(\boldsymbol{\theta}_t^{\otimes N})} \nabla \cdot \left(\pi(\boldsymbol{\theta}_t^{\otimes N}) (\bar{\mathbf{K}} \otimes \mathbf{I} + \sigma^2 \mathbf{I}) \right) + \sqrt{2\sigma^2 \mathbf{I}} d\mathbf{W}_{ND}, \quad (72)$$

where $\bar{\mathbf{K}}_{ij} = k(\boldsymbol{\theta}_i, \boldsymbol{\theta}_j)$. Formally, SPOS combines the SVGD particle update with a step of (multi-chained) Langevin diffusion. The SPOS particle update does not conform to the standard formulation of MCMC dynamics, yielding a biased sampling algorithm. However, such bias can be fixed by changing the diffusion coefficient into $\sqrt{2(\bar{\mathbf{K}} \otimes \mathbf{I} + \sigma^2 \mathbf{I})}$. Translating into discretized dynamics, SPOS generates samples from the target measure when the injected noise is correlated across particles. However, the correlated injected noise has variance approaching zero as $N \rightarrow \infty$.

2.7 Recovering SVGD with GFSF

While SVGD takes the form of gradient flow on $(\mathcal{P}(\Omega), W_{\mathcal{H}})$, we can connect SVGD with other form of smoothing discussed in Liu et al. (2019a), noted as gradient flow with smoothed test functions (GFSF). GSVGD taking $\mathbf{A} = \bar{\mathbf{K}} \otimes \mathbf{I}, \mathbf{C} = \mathbf{0}$ gives

$$\mathbf{v}^{\mathbf{A}, \mathbf{C}} = \bar{\mathbf{K}} \otimes \mathbf{I} \nabla \log \pi^{\otimes N} / \rho^{\otimes N} = \bar{\mathbf{K}} \otimes \mathbf{I} \nabla \log \pi^{\otimes N} - \bar{\mathbf{K}} \otimes \mathbf{I} \nabla \log \rho^{\otimes N}. \quad (73)$$

Using the GFSF estimation of $\nabla \log \rho$ ¹, the term $\overline{\mathbf{K}} \otimes \mathbf{I} \nabla \log \rho^{\otimes N}$ yields $\nabla \cdot \overline{\mathbf{K}}$, recovering the SVGD particle update. Viewing PARVI in the product space yields additional insights of connecting different smoothing methods. Analogously, we can use the generalized Stein’s identity (Gorham et al., 2019) to arrive at a GFSF smoothing of GSVGd.

3 Additional discussion

3.1 Formulating Riemannian Langevin diffusion as gradient flow on $(\mathcal{P}(\Omega), W_{2,\mathbf{A}})$

With $\mathbf{C} = \mathbf{0}$ and positive definite \mathbf{A} , we can generalize the 2-Wasserstein metric in the Benamou-Brenier form (Benamou and Brenier, 2000)

$$W_{2,\mathbf{A}}^2(\rho_0, \rho_1) = \inf_{\phi, \rho_t} \left\{ \int_0^1 \int \langle \nabla \phi_t, \mathbf{A} \nabla \phi_t \rangle dt : \dot{\rho}_t + \nabla \cdot (\rho_t \mathbf{A} \nabla \phi_t) = 0 \right\}. \quad (74)$$

The Onsager operator of $W_{2,\mathbf{A}}$ takes the form $G(\rho)^{-1} : \phi \mapsto -\nabla \cdot (\rho \mathbf{A} \nabla \phi)$. MCMC dynamics such as Riemannian Langevin diffusion (Girolami and Calderhead, 2011) can be interpreted as a gradient flow of KL $[\rho \parallel \pi]$ on $W_{2,\mathbf{A}}$: $\dot{\rho}_t = \nabla \cdot \left(\rho_t \mathbf{A} \nabla \frac{\delta \text{KL}[\rho_t \parallel \pi]}{\delta \rho_t} \right) = -G(\rho_t)^{-1} \frac{\delta \text{KL}[\rho_t \parallel \pi]}{\delta \rho_t}$, circumventing the necessity of defining a projection \mathfrak{p}_ρ onto the tangent space of $(\mathcal{P}(\Omega), W_2)$.

3.2 How to accelerate PARVI for underdamped Langevin diffusion?

Ma et al. (2019) argue that the underdamped Langevin diffusion with $\mathbf{A} = \begin{pmatrix} \mathbf{0} & \mathbf{0} \\ \mathbf{0} & \mathbf{AI} \end{pmatrix}$, $\mathbf{C} =$

$\begin{pmatrix} \mathbf{0} & -\mathbf{I} \\ \mathbf{I} & \mathbf{0} \end{pmatrix}$ is an analog of Nesterov’s acceleration of the overdamped Langevin diffusion $\mathbf{A} = \mathbf{I}$, $\mathbf{C} = \mathbf{0}$, and such analog still stands for their PARVI variants. Similar to results presented in MCMC research (Mou et al., 2021), we can construct PARVI with third-order Langevin diffusion $\mathbf{A} = \begin{pmatrix} \mathbf{0} & \mathbf{0} & \mathbf{0} \\ \mathbf{0} & \mathbf{0} & \mathbf{0} \\ \mathbf{0} & \mathbf{0} & \mathbf{AI} \end{pmatrix}$, $\mathbf{C} = \begin{pmatrix} \mathbf{0} & -\mathbf{I} & \mathbf{0} \\ \mathbf{I} & \mathbf{0} & -\gamma \mathbf{I} \\ \mathbf{0} & \gamma \mathbf{I} & \mathbf{0} \end{pmatrix}$, equivalent to applying a higher-order momentum method in gradient descent.

3.3 Momentum resampling

One unexplored aspect of particle variational inference with momentum variable is the possibility of turning PARVI into a proper sampling algorithm, one feat unattainable by de-randomization of LD, as deterministic optimization of N particle can only produce N samples. With the introduction of momentum variables, it is possible to periodically resample the momentum variable to obtain more samples from the target distribution – in practice, it involves combining the deterministic particle updates with a jump process that routinely samples from the marginal distribution of momentum.

Aside from possibly obtaining more samples, resampling during the optimization can also speed up convergence to the target distribution. As we know the marginal distribution with respect to \mathbf{r} , resampling of momentum variables reduces the KL-divergence between ρ_t and π , as $\text{KL}[\rho_t(\theta)\pi(\mathbf{r}) \parallel \pi(\theta)\pi(\mathbf{r})] \leq \text{KL}[\rho_t(\theta, \mathbf{r}) \parallel \pi(\theta)\pi(\mathbf{r})]$. It remains a theoretical and empirical open question whether resampling momentum can speed up convergence.

4 Experiment details

4.1 Toy experiments

The 2-dimensional likelihood of the toy experiments used in this paper takes the form of $\pi \propto \frac{1}{3} \sum_{i=1}^3 \exp\left(-\frac{x^4}{10} + \frac{(z_i y - x^2)^2}{2}\right)$, $z_i = \{-2, 0, 2\}$, and the original particle loca-

¹formally, GFSF is equivalent of applying the Stein gradient estimator (Li and Turner, 2017) without regularization.

tions are initialized as $\begin{pmatrix} x \\ y \end{pmatrix} \sim \mathcal{N}(0, 0.01\mathbf{I})$. We can use the energy function $U(\boldsymbol{\theta}) = \log\left(\frac{1}{3}\sum_{i=1}^3 \exp\left(-\frac{x^4}{10} + \frac{(z_i y - x^2)^2}{2}\right)\right)$ to construct Riemannian samplers in the experimental setting consistent with [Ma et al. \(2015\)](#), where Fisher information metric matrix is defined as $\mathbf{G}^{-1}(\boldsymbol{\theta}) = D\sqrt{|U(\boldsymbol{\theta}) + C|}$, $U = 1.5$, $C = 0.5$. In Riemannian Stein variational gradient descent (SVGD) ([Liu and Zhu, 2017](#)), we follow the practice of Riemannian LD ([Girolami and Calderhead, 2011](#)) and parametrize $\mathbf{A}(\boldsymbol{\theta}) = \mathbf{G}^{-1}(\boldsymbol{\theta})$, $\mathbf{C}(\boldsymbol{\theta}) = \mathbf{0}$; In Riemannian SGHMC, we follow ([Ma et al., 2015](#)) parametrize $\mathbf{A}(\boldsymbol{\theta}) = \begin{pmatrix} \mathbf{0} & \mathbf{0} \\ \mathbf{0} & \mathbf{G}^{-1}(\boldsymbol{\theta}) \end{pmatrix}$, $\mathbf{C}(\boldsymbol{\theta}) = \begin{pmatrix} \mathbf{0} & -\mathbf{G}^{-1/2} \\ \mathbf{G}^{-1/2} & \mathbf{0}(\boldsymbol{\theta}) \end{pmatrix}$.

4.2 Bayesian neural network experiments

In Bayesian neural network for regression, we use a standard structure of 1 hidden layers with width 50, along with a conjugate prior on the precision parameter of its weight priors. Specifically, we have

$$y \sim \mathcal{N}\left(\mathbf{W}_2^\top \text{ReLU}(\mathbf{W}_1^\top \mathbf{x} + \mathbf{b}_1) + \mathbf{b}_2, \gamma^{-1}\right), \quad (75)$$

$$\mathbf{W}_1, \mathbf{b}_1, \mathbf{w}_2, \mathbf{b}_2 \sim \mathcal{N}(\mathbf{0}, \lambda^{-1}\mathbf{I}), \mathbf{W}_1 \in \mathbb{R}^{D \times 50}, \mathbf{b}_1 \in \mathbb{R}^{50}, \quad (76)$$

$$\gamma, \lambda \sim \text{Gamma}(1, 0.1). \quad (77)$$

The weights \mathbf{W}_i are initialized with glort normal distribution and \mathbf{b}_i are initialized with zero.

The hyperparameters for the methods applied in the paper are selected by cross-validation in the following fashion: the learning rate η is selected in $\eta \in \{10^{-8}, 10^{-7}, 10^{-6}, 10^{-5}, 10^{-4}, 10^{-3}, 10^{-2}\}$; for methods involving additional momentum variables \mathbf{r} , we adopt the momentum interpretation of the underdamped Langevin dynamics ([Chen et al., 2014](#)) and select momentum term $\alpha \in \{0.01, 0.1, 0.5\}$ ²; for thermostat-type samplers, we additionally tune the precision parameter of the temperature variable, with $\mu \in \{0.1, 1.0, 10.0\}$. For methods involving kernel parameters, we parameterize a squared exponential kernel with the median method ([Liu and Wang, 2016](#)). We take symmetric splitting for methods involving momentum variables.

For the 6 datasets from UCI repository, we take a 90%/10% training/test partition of the data; for the 6 medium-sized datasets (except for “year” and “protein”), we take 20 different training / test splits, 6 splits for “protein”, and 6 different initializations with the “year” dataset, as the split is fixed. We implemented the models using JAX ([Bradbury et al., 2018](#)), and ran the experiments on Nvidia Volta V100 GPU nodes. We present the technical formulation of the methods and its running time in [Table 1](#) and [Table 2](#), respectively.

Method	A	C	π	hyperparameters	Reference
LD	\mathbf{I}	$\mathbf{0}$	$\pi(\boldsymbol{\theta})$	$\eta = \epsilon$	Welling and Teh (2011)
SVGD	\mathbf{I}	$\mathbf{0}$	$\pi(\boldsymbol{\theta})$	$\eta = \epsilon$	Liu and Wang (2016)
Blob	\mathbf{I}	$\mathbf{0}$	$\pi(\boldsymbol{\theta})$	$\eta = \epsilon$	Chen et al. (2018)
DE	-	-	$\pi(\boldsymbol{\theta})$	$\eta = \epsilon, \alpha$	Lakshminarayanan et al. (2017)
SGHMC-Blob	$\begin{pmatrix} \mathbf{0} & \mathbf{0} \\ \mathbf{0} & A\mathbf{I} \end{pmatrix}$	$\begin{pmatrix} \mathbf{0} & -\mathbf{I} \\ \mathbf{I} & \mathbf{0} \end{pmatrix}$	$\pi(\boldsymbol{\theta})\mathcal{N}(\mathbf{r} \mathbf{0}, \sigma^2\mathbf{I})$	$\eta = \epsilon^2\sigma^{-2}, \alpha = \epsilon\sigma^{-2}A$	Liu et al. (2019b)
SGHMC-Stein	$\begin{pmatrix} \mathbf{0} & \mathbf{0} \\ \mathbf{0} & A\mathbf{I} \end{pmatrix}$	$\begin{pmatrix} \mathbf{0} & -\mathbf{I} \\ \mathbf{I} & \mathbf{0} \end{pmatrix}$	$\pi(\boldsymbol{\theta})\mathcal{N}(\mathbf{r} \mathbf{0}, \sigma^2\mathbf{I})$	$\eta = \epsilon^2\sigma^{-2}, \alpha = \epsilon\sigma^{-2}A$	this work
SGNHT	$\begin{pmatrix} \mathbf{0} & \mathbf{0} & \mathbf{0} \\ \mathbf{0} & A\mathbf{I} & \mathbf{0} \\ \mathbf{0} & \mathbf{0} & \mathbf{0} \end{pmatrix}$	$\begin{pmatrix} \mathbf{0} & -\mathbf{I} & \mathbf{0} \\ \mathbf{I} & \mathbf{0} & (\mu\sigma^2)^{-1}\text{diag}(\mathbf{r}) \\ \mathbf{0} & -(\mu\sigma^2)^{-1}\text{diag}(\mathbf{r}) & \mathbf{0} \end{pmatrix}$	$\pi(\boldsymbol{\theta})\mathcal{N}(\mathbf{r} \mathbf{0}, \sigma^2\mathbf{I})\mathcal{N}(\boldsymbol{\xi} A\mathbf{1}, \mu^{-1}\mathbf{I})$	$\eta = \epsilon^2\sigma^{-2}, \alpha = \epsilon\sigma^{-2}A, \mu$	Ding et al. (2014)
SGNHT-Stein	$\begin{pmatrix} \mathbf{0} & \mathbf{0} & \mathbf{0} \\ \mathbf{0} & A\mathbf{I} & \mathbf{0} \\ \mathbf{0} & \mathbf{0} & \mathbf{0} \end{pmatrix}$	$\begin{pmatrix} \mathbf{0} & -\mathbf{I} & \mathbf{0} \\ \mathbf{I} & \mathbf{0} & (\mu\sigma^2)^{-1}\text{diag}(\mathbf{r}) \\ \mathbf{0} & -(\mu\sigma^2)^{-1}\text{diag}(\mathbf{r}) & \mathbf{0} \end{pmatrix}$	$\pi(\boldsymbol{\theta})\mathcal{N}(\mathbf{r} \mathbf{0}, \sigma^2\mathbf{I})\mathcal{N}(\boldsymbol{\xi} A\mathbf{1}, \mu^{-1}\mathbf{I})$	$\eta = \epsilon^2\sigma^{-2}, \alpha = \epsilon\sigma^{-2}A, \mu$	this work

Table 1: An overview of the parameters in the methods used in the BNN experiments paper, including the (possibly augmented) target distribution, the parameterizations of MCMC dynamics, and the tunable hyperparameters (step size η , momentum term α and precision term for the temperature variable μ).

4.3 Additional experiments

Apart from the standard from of GSVGD and Blob methods in the paper, we experimented Bayesian neural network with particle-based variational inference (PARVI) consistent with the pSGHMC-det

²It is notable that the step size ϵ in the discretization of dynamics does not directly correspond to the “effective learning rate” in SGHMC-type samplers.

	boston	concrete	energy	kin8nm	power	yacht	year	protein
LD	124.88(22.68)	91.40(45.34)	98.17(41.45)	131.89(21.67)	131.01(14.20)	86.91(42.83)	811.08(140.66)	559.76(9.84)
SVGD	75.76(10.04)	75.31(13.82)	67.70(19.69)	87.03(3.68)	81.98(10.59)	71.11(10.14)	704.39(30.75)	348.16(16.67)
Blob	79.69(2.25)	75.39(14.36)	66.79(19.86)	83.55(10.36)	75.35(18.10)	66.94(18.52)	708.06(16.48)	352.89(11.15)
HMC-Blob	76.76(20.62)	80.95(19.51)	83.31(16.53)	93.61(13.63)	87.99(16.13)	73.33(22.05)	874.68(165.39)	409.75(13.78)
SGNHT	231.86(55.61)	245.63(25.54)	252.53(3.79)	256.84(2.74)	232.18(60.56)	222.90(59.43)	1326.01(197.56)	1016.57(79.80)
DE	76.76(10.52)	75.53(14.57)	75.30(7.04)	80.76(13.80)	79.26(15.56)	70.80(13.89)	709.06(23.05)	351.96(13.21)
SGHMC-Stein	89.03(10.60)	91.82(8.58)	85.50(13.45)	95.02(9.94)	90.87(9.73)	81.02(16.11)	761.57(119.60)	395.49(14.61)
SGNHT-Stein	101.22(3.27)	94.33(13.16)	89.52(18.69)	86.18(19.88)	96.86(14.21)	89.98(13.62)	879.78(14.91)	429.61(13.22)

Table 2: Mean (standard deviation) of running times for BNN experiments measured in seconds. All methods are run for 5,000 iterations (first 6 columns, averaged over 20 runs) and 20,000 iterations (last 2 columns, averaged over 6 runs), respectively.

formula in [Liu et al. \(2019b\)](#), and the corresponding Stein version with reproducing kernel Hilbert space (RKHS) projection. The experiment results do not show clear difference from the standard form. From the perspective of Hamiltonian dynamics, we can view underdamped Langevin dynamics (LD) and this variant of PARVI both as Hamiltonian Monte Carlo with a “continuous resampling” of the momentum variable: underdamped LD resamples momentum by running overdamped LD on the momentum variable; its PARVI variant runs SVGD (Stein) or Blob variant as continuous resampling. While the particles do not converge to an equilibrium, the marginal distribution ρ_t remains unchanged.

	boston	concrete	energy	kin8nm	power	yacht	year	protein
SGHMC-Blob*	11.68(39.93)	0.21(0.45)	0.00(0.00)	0.07(0.00)	0.05(0.00)	0.00(0.00)	0.64(0.00)	0.49(0.01)
SGHMC-Stein*	0.12(0.07)	0.09(0.02)	0.00(0.00)	0.07(0.00)	0.05(0.00)	0.00(0.00)	0.65(0.00)	0.48(0.01)

Table 3: Mean (standard deviation) of mean squared error with PARVI experiment: the experimental setting is the same as the standard BNN experiment.

	boston	concrete	energy	kin8nm	power	yacht	year	protein
SGHMC-Blob*	-2.58(0.12)	-2.93(0.08)	-0.49(0.10)	1.23(0.02)	-2.77(0.04)	-0.70(0.36)	-3.58(0.00)	-2.87(0.01)
SGHMC-Stein*	-2.54(0.28)	-2.98(0.09)	-0.32(0.24)	1.25(0.02)	-2.78(0.03)	-0.76(0.53)	-3.59(0.00)	-2.87(0.01)

Table 4: Mean (standard deviation) of text log-likelihood with PARVI experiment: the experimental setting is the same as the standard BNN experiment.

References

- Richard Jordan, David Kinderlehrer, and Felix Otto. The variational formulation of the Fokker-Planck equation. *SIAM Journal on Mathematical Analysis*, 29(1):1–17, 1998.
- Charles Stein. A bound for the error in the normal approximation to the distribution of a sum of dependent random variables. *Proceedings of the Sixth Berkeley Symposium on Mathematical Statistics and Probability, Volume 2: Probability Theory*, 1972.
- Jackson Gorham, Andrew B. Duncan, Sebastian J. Vollmer, and Lester Mackey. Measuring sample quality with diffusions. *Annals of Applied Probability*, 29(5):2884–2928, 2019.
- Qiang Liu and Dilin Wang. Stein variational gradient descent: A general purpose Bayesian inference algorithm. In *Advances in Neural Information Processing Systems*, volume 29, pages 2378–2386, 2016.
- Víctor Gallego and David Ríos Insua. Stochastic gradient MCMC with repulsive forces. *arXiv preprint arXiv:1812.00071*, 2018.
- Jianyi Zhang, Ruiyi Zhang, Lawrence Carin, and Changyou Chen. Stochastic particle-optimization sampling and the non-asymptotic convergence theory. In *International Conference on Artificial Intelligence and Statistics*, pages 1877–1887, 2020.
- Chang Liu, Jingwei Zhuo, Pengyu Cheng, Ruiyi Zhang, and Jun Zhu. Understanding and accelerating particle-based variational inference. In *International Conference on Machine Learning*, pages 4082–4092, 2019a.
- Yingzhen Li and Richard E. Turner. Gradient estimators for implicit models. In *International Conference on Learning Representations*, 2017.
- Jean-David Benamou and Yann Brenier. A computational fluid mechanics solution to the Monge-Kantorovich mass transfer problem. *Numerische Mathematik*, 84(3):375–393, 2000.
- Mark Girolami and Ben Calderhead. Riemann manifold langevin and hamiltonian monte carlo methods. *Journal of The Royal Statistical Society Series B-statistical Methodology*, 73(2):123–214, 2011.
- Yi-An Ma, Niladri S. Chatterji, Xiang Cheng, Nicolas Flammarion, Peter L. Bartlett, and Michael I. Jordan. Is there an analog of Nesterov acceleration for MCMC. *arXiv preprint arXiv:1902.00996*, 2019.
- Wenlong Mou, Yi-An Ma, Martin J. Wainwright, Peter L. Bartlett, and Michael I. Jordan. High-order Langevin Diffusion yields an accelerated MCMC algorithm. *Journal of Machine Learning Research*, 22(42):1–41, 2021.
- Yi-An Ma, Tianqi Chen, and Emily B. Fox. A complete recipe for stochastic gradient MCMC. In *NIPS’15 Proceedings of the 28th International Conference on Neural Information Processing Systems - Volume 2*, volume 28, pages 2917–2925, 2015.
- Chang Liu and Jun Zhu. Riemannian Stein variational gradient descent for bayesian inference. In *AAAI*, pages 3627–3634, 2017.
- Tianqi Chen, Emily Fox, and Carlos Guestrin. Stochastic gradient Hamiltonian Monte Carlo. In *International conference on machine learning*, pages 1683–1691, 2014.
- James Bradbury, Roy Frostig, Peter Hawkins, Matthew James Johnson, Chris Leary, Dougal Maclaurin, George Necula, Adam Paszke, Jake VanderPlas, Skye Wanderman-Milne, and Qiao Zhang. JAX: composable transformations of Python+NumPy programs, 2018. URL <http://github.com/google/jax>.
- Max Welling and Yee W. Teh. Bayesian learning via stochastic gradient Langevin dynamics. In *Proceedings of the 28th International Conference on Machine Learning*, pages 681–688, 2011.
- Changyou Chen, Ruiyi Zhang, Wenlin Wang, Bai Li, and Liqun Chen. A unified particle-optimization framework for scalable Bayesian sampling. In *UAI*, pages 746–755, 2018.

- Balaji Lakshminarayanan, Alexander Pritzel, and Charles Blundell. Simple and scalable predictive uncertainty estimation using deep ensembles. In *Advances in Neural Information Processing Systems*, volume 30, pages 6402–6413, 2017.
- Chang Liu, Jingwei Zhuo, and Jun Zhu. Understanding MCMC dynamics as flows on the Wasserstein space. In *International Conference on Machine Learning*, pages 4093–4103, 2019b.
- Nan Ding, Youhan Fang, Ryan Babbush, Changyou Chen, Robert D Skeel, and Hartmut Neven. Bayesian sampling using stochastic gradient thermostats. In *Advances in Neural Information Processing Systems 27*, volume 27, pages 3203–3211, 2014.